



Seasonal to interannual variability of the Pacific water boundary current in the Beaufort Sea



Eric T. Brugler^a, Robert S. Pickart^{a,*}, G.W.K. Moore^b, Steven Roberts^c, Thomas J. Weingartner^c, Hank Statscewich^c

^a Woods Hole Oceanographic Institution, Woods Hole, MA 02540, USA

^b University of Toronto, Toronto, ON M5S 1A1, Canada

^c University of Alaska Fairbanks, Fairbanks, AK 99775, USA

ARTICLE INFO

Article history:

Received 22 October 2013

Received in revised form 2 May 2014

Accepted 3 May 2014

Available online 17 May 2014

ABSTRACT

Between 2002 and 2011 a single mooring was maintained at the core of the Pacific water boundary current in the Beaufort Sea, approximately 150 km east of Pt. Barrow, Alaska. Using velocity and hydrographic data from six year-long deployments, we examine the variability of the current on seasonal to interannual timescales. The seasonal signal is characterized by enhanced values of volume, heat, and freshwater transport during the summer months associated with the presence of two summertime Pacific water masses, Alaskan Coastal Water and Chukchi Summer Water. Strikingly, over the decade the volume transport of the current has decreased by more than 80%, with comparable reductions in the heat and freshwater transports, despite the fact that the flow through Bering Strait has increased over this time period. The largest changes in the boundary current have occurred in the summer months. Using atmospheric reanalysis fields and weather station data, we demonstrate that an increase in summer easterly winds along the Beaufort slope is the primary cause for the reduction in transport. The stronger winds are due to an intensification of the summer Beaufort High and deepening of the summer Aleutian Low. Using additional mooring and shipboard data in conjunction with satellite fields, we investigate the implications of the reduction in transport of the boundary current. We argue that a significant portion of the mass and heat passing through Bering Strait in recent years has been advected out of Barrow Canyon into the interior Canada Basin – rather than entering the boundary current in the Beaufort Sea – where it is responsible for a significant portion of the increased sea ice melt in the basin.

© 2014 Elsevier Ltd. All rights reserved.

Introduction

Pacific water flowing northward through Bering Strait has profound impacts on the physical state and ecosystem of the Western Arctic Ocean. The cold, dense water fluxed northward in winter and spring ventilates the upper halocline (Aagaard et al., 1981) and provides nutrients that fuel primary production each year (e.g. Codispoti et al., 2005). The warm Pacific water penetrating northward in summer and fall helps to melt back the seasonal ice cover (Weingartner et al., 2005a) and is contributing to the decline of the perennial ice pack (e.g. Steele et al., 2010). The summer water also supplies a significant quantity of freshwater to the Beaufort Gyre (Yang, 2006; Pickart et al., 2013a). As such, it is important to determine the pathways, mechanisms, and

timescales by which the Pacific water penetrates the Arctic domain, and how these are changing in a warming climate.

The yearly average northward transport of Pacific water through Bering Strait is 0.8 Sv (Roach et al., 1995). After entering the Chukchi Sea the flow divides into three branches due the topography of the shelf (Fig. 1) (Weingartner et al., 2005a). Upon reaching the edge of the Chukchi Sea some of the water is channeled eastward and flows as a narrow shelfbreak jet in the Beaufort Sea (Pickart, 2004; Nikolopoulos et al., 2009). Farther down the slope Atlantic water also flows eastward as part of the large-scale cyclonic boundary current system of the Arctic Ocean (Rudels et al., 1994; Woodgate et al., 2001; Karcher et al., 2007; Aksenov et al., 2011). There is a pronounced seasonality of the Pacific water current. In summertime the flow is surface-intensified and advects two types of summer water masses (von Appen and Pickart, 2012). From early fall through winter the flow is bottom-intensified and the predominant water mass transported by the current is remnant winter water (Nikolopoulos et al., 2009). Finally, during spring and early summer, newly-ventilated Pacific winter water is

* Corresponding author. Address: Woods Hole Oceanographic Institution, 266 Woods Hole Rd., Clark 359B, (MS# 21), Woods Hole, MA 02543-1050, USA. Tel.: +1 508 289 2858.

E-mail address: rpickart@whoi.edu (R.S. Pickart).

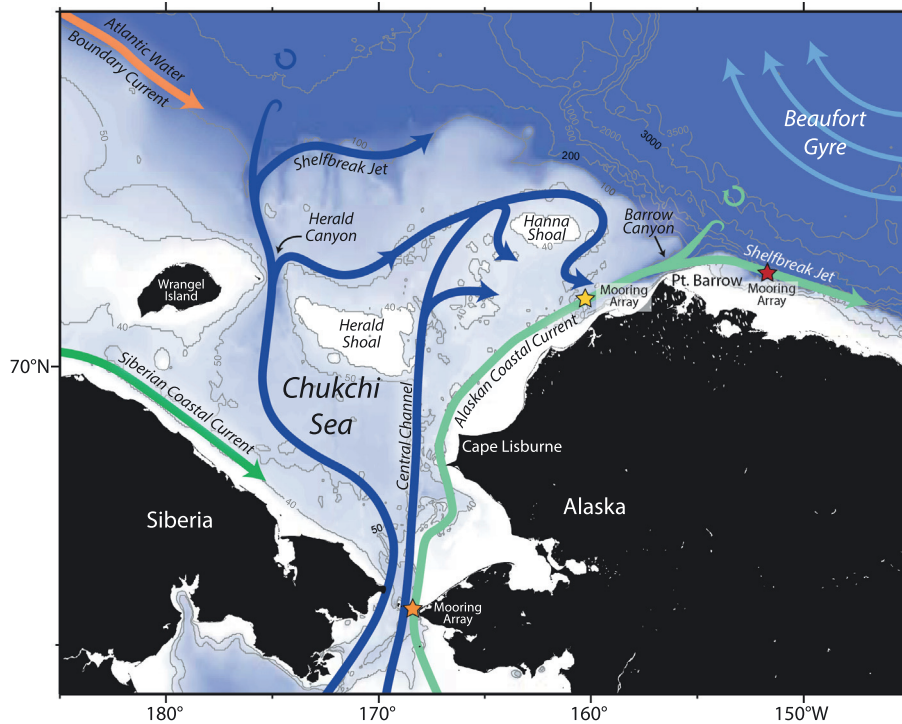


Fig. 1. Schematic showing the major currents in the Chukchi and Beaufort Seas and the geographical place names for the region. The location of the Beaufort slope mooring array is indicated by the red star, the Barrow Canyon mooring array is indicated by the yellow star, and the Bering Strait mooring array is indicated by the orange star. (For interpretation of the references to color in this figure legend, the reader is referred to the web version of this article.)

advected in a bottom-intensified jet (Spall et al., 2008). While these seasonal configurations seem to occur each year, the variation in timing and spatial distribution of the different water masses from year to year is presently unknown.

In order to accurately determine how the Pacific water impacts the Arctic system, it is necessary to understand the detailed structure and variability of the shelfbreak jet. Not only is the current the major conduit by which Pacific water exits the Chukchi Sea, but it represents the interface between the shelf and the Arctic Ocean interior. Exchange across the Beaufort shelfbreak occurs in two ways: through hydrodynamic instability of the boundary current (Spall et al., 2008; von Appen and Pickart, 2012), and via wind-forcing. The shelfbreak jet is both baroclinically and barotropically unstable and is known to spawn eddies that transport Pacific water offshore. Such eddies are found throughout the interior Canada Basin (Plueddemann, 1999). Upwelling driven by easterly winds is common and occurs in all seasons and under varying ice conditions (Schulze and Pickart, 2012). Pickart et al. (2013b) showed that a single strong storm can result in a substantial off-shelf flux of heat and freshwater, and a significant on-shelf transport of nutrients. The salt, nutrients, and zooplankton brought to the shelves via upwelling are thought to play an important role in the productivity and state of the local ecosystem (Pickart et al., 2013b). Such storms are also thought to release a significant amount of CO₂ to the atmosphere (Mathis, 2012).

For much of the past decade the Pacific water boundary current has been measured using moorings in the Alaskan Beaufort Sea, deployed roughly 150 km to the east of Pt. Barrow. The main goal of this paper is to use these data to quantify both the seasonal and interannual variability of the current over this time frame, and to investigate the physical drivers responsible for these changes. We begin with a description of the mean state of the current and a characterization of the water masses that it advects. The seasonal signal is then quantified, followed by an investigation of the

interannual variability. Next we describe the large-scale atmospheric conditions during the study period, and then consider the local wind forcing, lateral boundary conditions, and sea ice concentration near the mooring site. We find that profound changes have occurred in the Pacific water boundary current over the last 10 years, much of which can be explained by atmospheric forcing. Finally, we discuss how these changes in the current can divert heat away from the shelf edge and contribute to ice melt in the interior Canada Basin.

Data

Mooring array data from 2002 to 2004

An array of 8 moorings was deployed across the Beaufort shelfbreak and slope near 152°W as part of the Western Arctic Shelf-Basin Interactions (SBI) program from 2002 to 2004 (Fig. 2). The array was aligned perpendicular to the local bathymetry, and the moorings were spaced 5–10 km apart. The moorings were named BS1–BS8 (onshore to offshore), although the shoreward-most mooring is not considered in this study. Hydrographic variables on moorings BS2–BS6 were measured using a motorized conductivity-temperature-depth (CTD) profiler known as a Coastal Moored Profiler (CMP). The CMPs provided vertical traces over a nominal depth range of 40 m to just above the bottom 2–4 times a day with a vertical resolution of 2 m. To measure velocity, upward-facing acoustic Doppler current profilers (ADCPs) were used for moorings BS2–BS6. The ADCPs provided hourly profiles of velocity with a vertical resolution of 5–10 m. Moorings BS7 and BS8 used McLane moored profilers (MMPs) for measuring the hydrographic variables, and acoustic travel-time current meters (attached to the MMPs) for measuring the velocity. The reader is referred to Spall et al. (2008) and Nikolopoulos et al. (2009) for a

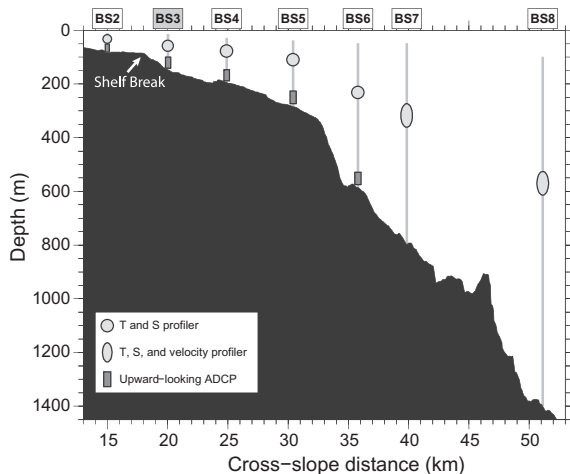


Fig. 2. The SBI mooring array deployed across the Beaufort shelfbreak and slope from 2002 to 2004 near 152°W. The instruments used on each mooring are identified in the key. The shelfbreak is located approximately 70 km offshore of the coastline. The shelfbreak mooring (BS3) is highlighted gray.

detailed description of the hydrographic and velocity measurements, respectively, including a discussion of the calibration and accuracy of the sensors.

For the present analysis we use data from moorings BS2 to BS6, which measured temperature and salinity every 6 h and velocity hourly. In particular, we employ the same data product used by von Appen and Pickart (2012) who constructed vertical sections of the hydrographic and velocity data at each time step. The sections were gridded using Laplacian-spline interpolation with a grid spacing of 2 km in the horizontal and 10 m in the vertical. Since the present study focuses on the Pacific water masses, the domain is restricted to the upper 300 m.

Mooring data from 2005 to 2011

A year after the conclusion of the SBI program, a single mooring was re-deployed in the Beaufort shelfbreak current as part of a series of three separate field programs. The mooring in question was BS3, located just offshore of the shelfbreak in 147 m of water. (From hereon, BS3 will be referred to as the "shelfbreak mooring".) The rationale for this was provided by Nikolopoulos et al. (2009) who determined that the vertically integrated velocity from the shelfbreak mooring alone was highly correlated with the transport of the full boundary current. To date, the shelfbreak mooring has been deployed seven times between August 2002 and October 2012, with each deployment lasting for about one year (the most recent deployment is not used here because the data were still being processed at the time of the analysis). Subsequent to the SBI program, the hydrographic data at the shelfbreak mooring were obtained using a CMP, and the velocity data collected using one or two upward-facing ADCPs. Each deployment varied slightly in length, start date, end date, data coverage, vertical resolution, and instrumentation. Table 1 provides general information

regarding each deployment. The reader is referred to Brugler (2013) for a detailed description of the instrument configuration and data processing for each individual deployment.

Meteorological timeseries

Wind data used in the study come from the meteorological station located in Pt. Barrow, Alaska, which is approximately 150 km to the west of the Beaufort slope mooring site (Fig. 1). It has been demonstrated previously that the wind record at this location is a good proxy for the winds near 152°W (Nikolopoulos et al., 2009; Pickart et al., 2011). The data were acquired from the National Climate Data Center of the National Oceanic and Atmospheric Administration (NOAA) and subject to a set of routines to remove erroneous values and interpolate small gaps of less than 6 h (see Pickart et al., 2013b for details). Nikolopoulos et al. (2009) determined that alongcoast winds (105°T) are most strongly correlated with the flow of the Beaufort shelfbreak jet. Consequently, we use the alongcoast component of the wind velocity in this study, where positive refers to westerly winds and negative to easterly winds.

Atmospheric reanalysis fields

Reanalysis fields are used to investigate the large-scale meteorological context over the time period of the mooring records. We employ the high-resolution data set known as the North American Regional Reanalysis (NARR, Mesinger et al., 2006). The space and time resolution of the NARR product is 32 km and 3 h, respectively. The NARR product utilizes newer data assimilation and modeling advances that have been developed subsequent to the original National Centers for Environmental Prediction (NCEP) global reanalysis product. The present study uses the NARR sea level pressure data and 10 m winds for the region shown in Fig. 12. The NARR data were validated against the Barrow wind timeseries in Brugler (2013).

Sea-ice concentration data

The sea-ice concentration data used in the study are a blended product combining Advanced Very High Resolution Radiometer (AVHRR) data and the Advanced Microwave Scanning Radiometer-Earth Observing System (AMSR-E) data. The record extends from 2002 to 2011, which is the timeframe that the AMSR-E obtained measurements onboard the National Aeronautics and Space Administration's (NASA) Aqua satellite. NOAA constructed this product in real-time following Grumbine (1996) and then later adjusted and corrected it following Cavalieri et al. (1999). The accuracy of the sea ice concentration is estimated to be ±10% (Cavalieri et al., 1991). The AVHRR-AMSR product is provided once per day at a spatial resolution of 0.25° (Reynolds et al., 2007).

Satellite imagery

Satellite-derived sea surface temperature (SST) and visible imagery used in the study were based on data collected from the high-resolution Moderate Resolution Imaging Spectroradiometer

Table 1
Shelfbreak mooring deployments.

Deployment	Location	Depth (m)	Start date	End date
2002–2003	71°23.69'N 152°5.88'W	147	01-August-2002	28-September-2003
2003–2004	71°23.69'N 152°2.81'W	147	06-October-2003	11-September-2004
2005–2006	71°23.73'N 152°2.14'W	147	06-August-2005	13-August-2006
2008–2009	71°24.09'N 152°2.82'W	147	13-August-2008	29-July-2009
2009–2010	71°23.63'N 152°3.82'W	147	04-August-2009	15-September-2010
2010–2011	71°23.65'N 152°2.81'W	147	16-September-2010	11-October-2011

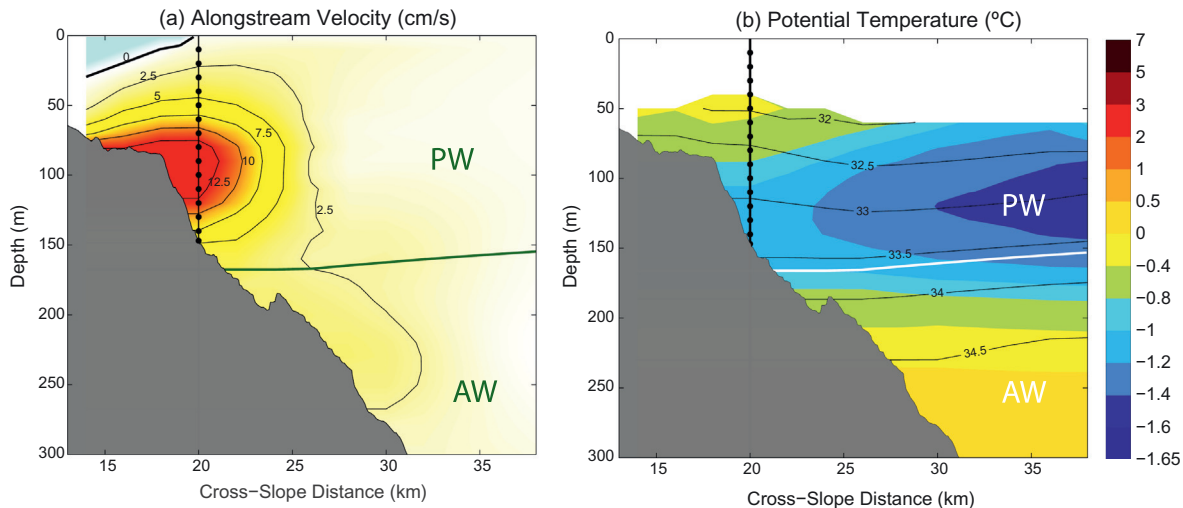


Fig. 3. Vertical sections of (a) mean alongstream velocity (cm/s) and (b) mean potential temperature (color) and salinity (contours) for the year of August 2002–July 2003. The thick green/white line is the 33.64 isohaline, which denotes the mean interface between the Atlantic and Pacific water as determined by Nikolopoulos et al. (2009). (For interpretation of the references to color in this figure legend, the reader is referred to the web version of this article.)

(MODIS) sensor onboard NASA's polar orbiting satellites Aqua and Terra. MODIS visible imagery was obtained from <http://lance-modis.eosdis.nasa.gov/imagery/subsets/?mosaic=Arctic> and MODIS SST imagery was retrieved from <http://oceancolor.gsfc.nasa.gov/cgi/browse.pl?sen=am>. The images are composites of sea surface temperature and visible imagery and have a spatial resolution of 250 m.

Shipboard hydrographic and velocity data

Shipboard data obtained from the Chukchi Sea in 2011 are used in the study. In July 2011 the United States Coast Guard Cutter (USCGC) *Healy* occupied a transect across the Chukchi Sea continental slope to the west of Barrow Canyon. Expendable CTDs (XCTDs) were dropped approximately every 5 km while the ship steamed at 10 knots, and the vessel-mounted ADCP collected data continuously during the transect. The accuracy of the XCTD is taken to be 0.02 °C for temperature, 0.04 for salinity, and 1 m for depth (see Kadko et al., 2008). The vessel-mounted ADCP data from Healy's Ocean Surveyor 150 kHz instrument were collected using the University of Hawaii's UHDAS software and subsequently processed using the CODAS3 software package (see <http://currents.soest.hawaii.edu>). Following this, the velocities were de-tided using the Oregon State University model (<http://volkov.oce.orst.edu/tides>; Padman and Erofeeva, 2004). The accuracy of the final de-tided velocities is estimated to be ±2 cm/s.

Methods

Shelfbreak mooring transport proxy

The SBI mooring array located at 152°W measured the Pacific Arctic boundary current for two consecutive years, 2002–2004. Using the full suite of hydrographic and velocity data, Nikolopoulos et al. (2009) demonstrated that the current is trapped to the shelfbreak throughout the year and that the dominant variability is due to pulsing of the flow, rather than meandering of the current. This suggests that a single mooring placed near the shelfbreak should be able to capture the main transport signal of the Pacific water, which is generally confined to the upper 150 m of the water column. Fig. 3a shows the mean structure of the current from 1 August 2002 to 31 July 2003. The black vertical line indicates the location of the shelfbreak mooring and the solid

circles represent the gridded velocity measurements. Using the data from the first year we constructed a proxy for the volume transport of the full current using only the shelfbreak mooring measurements.¹ This is subsequently used to analyze the interannual variability of the current.

The first step in devising the proxy was to choose a time invariant width of the current, which is a function of depth (i.e. vertical bin). Two metrics were considered in the choice of the widths. The first criterion was to minimize the root mean square (rms) difference between the full SBI array transport and the shelfbreak mooring proxy transport, and the second criterion was to minimize the difference in the record-length mean of the two transports. For each bin we chose the width that best met these two criteria jointly. We note that the transport measurements are restricted to the upper 147 m of the water column because the shelfbreak mooring only measured to this depth. However, Nikolopoulos et al. (2009) demonstrated that the mean interface between the Pacific water and Atlantic water at this location corresponds to a salinity of 33.64. As seen in Fig. 3, the shelfbreak mooring captures most of the Pacific-origin water. Using the full array data it was determined that the upper 150 m annually accounted for 91% of the volume transport, 97% of the heat transport, and 98% of the freshwater transport of Pacific water.

The transport proxy was further refined to account for two different types of current behavior that resulted in systematic discrepancies between the full transport and the estimate from the single mooring. During summer, the Pacific water jet is surface-intensified, and, as such, is not as strongly constrained by the bottom topography. Consequently there are times when the jet meanders offshore of the shelfbreak. In these instances the proxy underestimates the true transport. In the fall and winter months, during upwelling events, the flow in the vicinity of the shelfbreak (i.e. the core of the jet) does not reverse as readily as the seaward part of the current. At these times the proxy overestimates the transport of the actual jet. Fortunately, by considering the full SBI array data, we were able to establish objective procedures to mitigate each of these scenarios and increase the accuracy of the proxy. First, we used the potential temperature data and the computed value of the stratification at the shelfbreak site to identify when the current shifted offshore, and then statistically

¹ The second year of data were not used to construct the proxy because of a data gap in the upper portion of the water column at the shelfbreak mooring.

determined an effective adjustment. Second, we applied a graphical user interface to identify upwelling events and subsequently applied an “average storm” correction. These procedures are described in detail in Brugler (2013). We note, however, that the use of these adjustments resulted in only minor quantitative differences.

The resulting proxy transport timeseries for year 1, after applying the depth-varying width and incorporating the corrections for the occasional meanders and upwelling events, is compared with the full transport of the Pacific water boundary current in Fig. 4. One sees that the agreement is excellent ($r = .92$). The year-long mean full transport is 0.114 Sv, while that of the proxy is 0.123 Sv. The rms difference between the two timeseries is 0.20 Sv, with the proxy slightly underestimating the true variability of the current (the range of the transport is ~ 4 Sv).

Gridding the shelfbreak mooring data

The mooring hydrographic and velocity data were interpolated onto a regular depth/time grid which was used for part of the analysis. First the velocity data were rotated into a coordinate frame dictated by the direction of the depth-averaged flow and the principal axis variance ellipses, following Nikolopoulos et al. (2009). The positive x (alongstream) direction is 120°T , which is nearly parallel to the local bathymetry, and the positive y direction (cross-stream) is 30°T . These are slightly different (by 5°) than the directions determined by Nikolopoulos et al. (2009) who used only the first year of data. The velocities were then low passed using a second order Butterworth filter with a cut-off period of 36 h. This effectively removed both the tidal (semi-diurnal and diurnal) and inertial signals, which were small to begin with (see Pickart et al., 2013b). Following this, both the hydrographic (potential temperature, salinity, potential density) and velocity data were gridded using a 2-D Laplacian-spline interpolation scheme with a vertical spacing of 10 m and temporal grid spacing of 3 h. The velocity grid extended from 10 to 150 m, while the hydrographic grid extended from 50 to 130 m (since the CMP sampled a smaller part of the water column).

Transport calculations

Volume transport

The volume flux of the Pacific water shelfbreak jet at each point in time is given by

$$Q = \int_A v(x, z) dA, \quad (1)$$

where $v(x, z)$ is the alongstream velocity and A is the cross-sectional area of the current. We also consider the volume flux of the individual Pacific-origin water masses (i.e. summer and winter waters). To do this it was necessary to extrapolate the hydrographic variables upward to the surface and downward to the bottom, which was done using constant extrapolation. The volume flux timeseries for each water mass was then constructed by identifying which grid cells contained the water mass in question for each time step, and summing accordingly.

Heat transport

The transport of heat is given by

$$H = \int_A (v(x, z)(\rho)(\theta - \theta_0)(C_p)) dA, \quad (2)$$

where ρ is the in situ density, θ is the potential temperature, and C_p is the specific heat of seawater. Following earlier studies in the Pacific Arctic (e.g. Woodgate et al., 2010), we compute the heat flux relative to a reference temperature $\theta_0 = -1.91^\circ\text{C}$ (the freezing point of Bering Strait waters), hence it reflects the amount of heat available to melt sea-ice.

The hydrographic variables in (2) were extrapolated uniformly from the uppermost bin to the surface and from the deepest bin to the bottom. Since the heat flux is dominated by the summer waters, which are warmest near the surface, the use of constant extrapolation leads to an underestimate of the heat transport. The impact of the extrapolation was assessed as follows. During the 2005–2006 deployment, the shelfbreak mooring contained two moored profilers. The lower profiler was the CMP which profiled from 130 m to 45 m depth, and the upper profiler was a

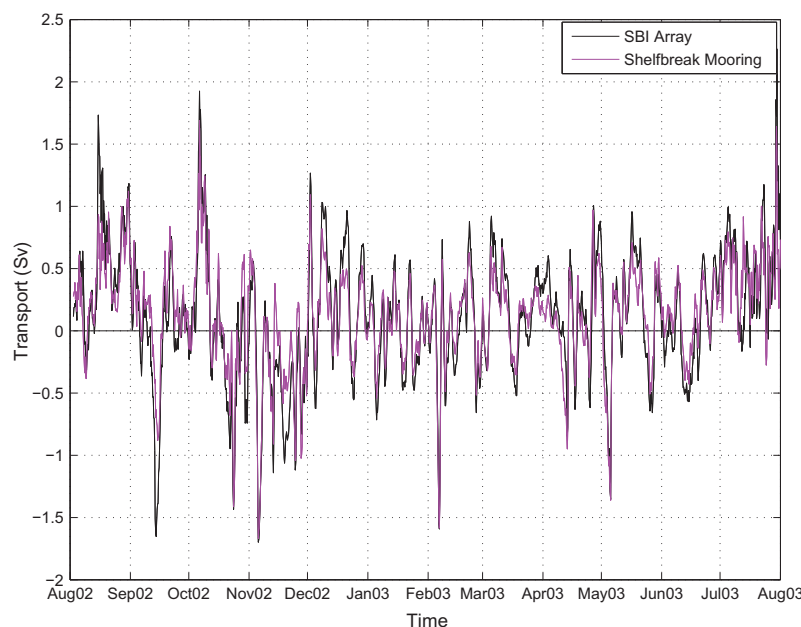


Fig. 4. Timeseries of daily transport calculated for the full SBI array (black) and the shelfbreak mooring proxy (purple). The correlation between the two timeseries is $r = .92$. (For interpretation of the references to color in this figure legend, the reader is referred to the web version of this article.)

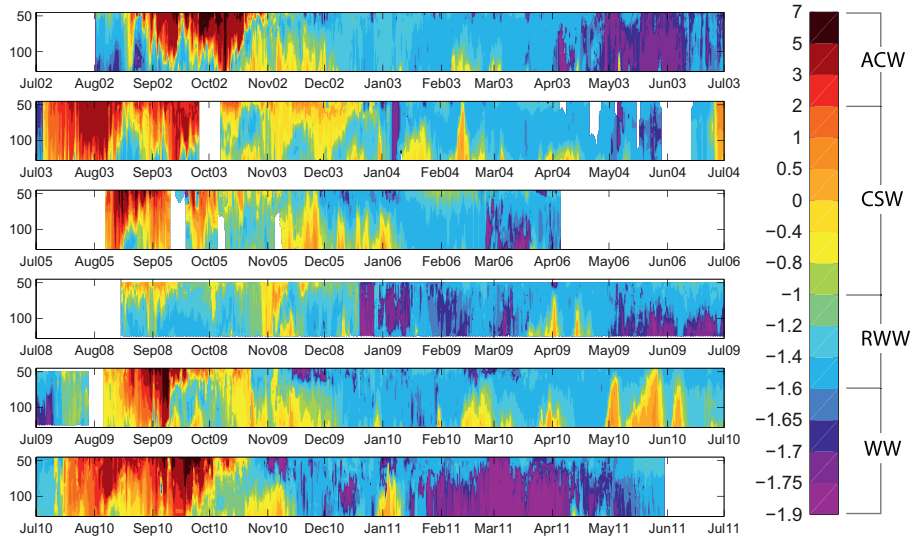


Fig. 5. Depth/time plot of potential temperature ($^{\circ}\text{C}$) at the shelfbreak mooring (in the core of the boundary current) from 45 to 130 m depth. The different Pacific water masses are indicated adjacent to the color bar. (For interpretation of the references to color in this figure legend, the reader is referred to the web version of this article.)

coastal winched profiler (CWP) that sampled from 40 m to just below the sea surface (Pickart et al., 2013a). The two profilers together provided hydrographic vertical profiles for nearly the full water column at 2 m resolution. We found that the heat transport calculated using constant extrapolation was on average 80% of that calculated using the dual profiler data for the 2005–2006 deployment. This underestimate should be kept in mind when considering the results presented below.

Freshwater transport

Following earlier studies, we compute the freshwater flux anomaly (hereafter simply called the freshwater flux) relative to a reference salinity

$$F = \int_A \left(v(x, z) \left(1 - \frac{S(x, z)}{S_0} \right) \right) dA, \quad (3)$$

where S is the salinity, and S_0 is the reference salinity taken to be the Arctic mean value of 34.8 (Aagaard and Carmack, 1989). Again, we used the CWP data to assess the impact of using constant extrapolation of salinity to the surface. We found that the freshwater transport calculated using constant extrapolation was 83% of that calculated using data from the full water column for the 2005–2006 deployment. Therefore, the bias in freshwater flux is comparable to that for the heat flux.

The Pacific water shelfbreak current

Water mass constituents

Over the course of a year, five water masses are advected by the shelfbreak current in the Alaskan Beaufort Sea. Fig. 5 shows the marked variation in potential temperature at the core of the jet. While there is clear seasonality, the exact timing of the water masses within the boundary current varies from year to year. Warm Alaskan Coastal Water (ACW) is present at various times between July and early October (this water mass is also referred to as Eastern Chukchi Summer Water, see Shimada et al. (2001)). The ACW is transported to the Beaufort Sea by the Alaskan Coastal Current (ACC), which emanates from the easternmost branch of Bering Strait outflow.² The water is very warm and fresh, with

temperatures greater than 2°C and salinities between 30 and 33.64 (Fig. 6). It is formed as a result of river runoff in the Gulf of Alaska and Bering Sea (Weingartner et al., 2005b). Note in Fig. 5 the different arrival times and quantities of ACW each year. For example, in 2003 ACW is present for three months of the year, whereas in 2009 it is there for only about a month. Interestingly, in 2008 there is no sign of ACW after mid-August, yet in every other year there were large amounts of ACW present beyond this date.

The second Pacific summer water mass transported by the shelfbreak jet is known variously as Chukchi Summer Water (CSW, von Appen and Pickart, 2012), Summer Bering Sea Water (Steele et al., 2004), and Western Chukchi Summer Water (Shimada et al., 2001). Here we refer to it as CSW, and define it to be water with temperatures between -1°C and 2°C and salinities between 30 and 33.64 (Fig. 6). CSW is cooler, saltier, and less stratified than ACW, and is generally found in the Beaufort shelfbreak current in early summer and again in early fall (i.e. bracketing the presence of ACW, von Appen and Pickart (2012)). However, it can be present nearly any time of the year (for instance it was observed in February 2006 near 50 m depth, Fig. 5).

Two different types of Pacific winter water are advected by the boundary current. The first is referred to as newly ventilated Winter Water (WW), which is weakly stratified and colder than -1.6°C and has salinities between 30 and 35. Its characteristics are close to the water entering Bering Strait during the winter months, formed via convection in the Bering Sea (e.g. Muench et al., 1988). It is the coldest water mass found in the Beaufort shelfbreak jet and generally appears in late-winter into spring. However, this varies significantly from year to year (Fig. 5). Several factors seem to be responsible for this variability, including changes in the Bering Strait inflow, atmospheric forcing, and sea ice cover/polynya activity (Itoh et al., 2012). The second cold Pacific water mass is Remnant Winter Water (RWW), which is winter water that has been modified by a combination of lateral mixing and atmospheric heating after its formation. RWW is defined as water with temperatures generally between -1.6°C and -1°C and salinities ranging from 30 to 33.64 (Fig. 6). It can appear in the shelfbreak current in every month of the year, including summer.

In addition to the Pacific-origin waters, Atlantic Water (AW) is advected by the boundary current. Following Nikolopoulos et al. (2009) we define this to be water with salinities exceeding 33.64 and temperatures greater than -1.26°C . AW is transported eastward along the Beaufort slope by the Arctic-wide cyclonic

² The Beaufort shelfbreak jet can be considered as the eastward extension of the ACC during the time period that it advects ACW.

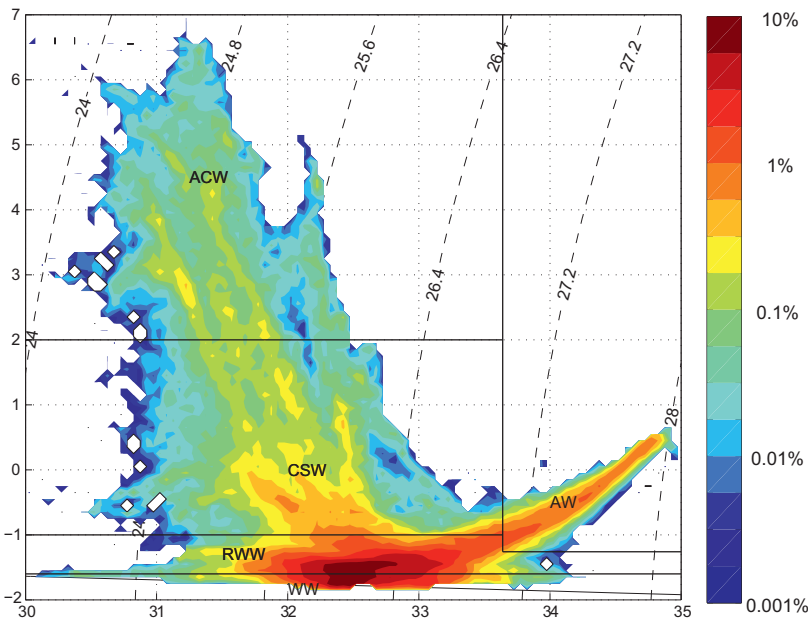


Fig. 6. T-S diagram showing the occurrence of the different water masses measured during the six deployments of the shelfbreak mooring. Units are percentage of all measurements per $0.1\text{ }^{\circ}\text{C}$ and 0.05 salinity (note the logarithmic scale). The black lines delimit the five water masses. ACW = Alaskan Coastal water; CSW = Chukchi summer water; WW = Winter water; RWW = Remnant winter water; AW = Atlantic water.

boundary current system, which is not considered as part of the shelfbreak jet (there is a minimal contribution in transport to the deepest part of the jet, see Nikolopoulos et al. (2009)). However, the frequent easterly winds in the region cause the shelfbreak current to reverse and Atlantic Water to be upwelled to the vicinity of the shelfbreak. These events are evident in Fig. 5 as the warm spikes emanating from depth (e.g. in December 2005).

Fig. 6 displays the five water masses in temperature-salinity space and indicates their relative occurrence in the core of the boundary current over the 6-year period of the study. The two types of winter water (RWW and WW) appear most frequently in the current, while CSW is more commonly found than ACW. The high percentage of AW attests to the frequent occurrence of upwelling in the region.

Mean structure

As noted above (Fig. 3), the Pacific water boundary current is centered near the shelfbreak at approximately 100 m depth. The year-long mean fields from the first deployment (2002–2003) suggest that the current is 10–15 km wide, with Pacific summer water near the shelfbreak in the upper 100 m, a layer of Pacific winter water between 100–150 m, and relatively warm and salty AW below this. In the mean it is hard to distinguish ACW from CSW because the former is only present a few months of the year and gets averaged out. Similarly, the two winter waters, RWW and WW, are not distinguishable in the year-long average due to the relatively sporadic occurrence of WW.

The mean vertical structure at the current core, using the full six years of data, is consistent with the first year mean section (Fig. 7). Relatively warm, fresh Pacific summer water resides above 100 m, with cooler, saltier Pacific winter waters below this. The 6-year mean alongstream velocity profile shows a peak of approximately 10 cm/s between 80 and 100 m. Note that this is smaller than the mean core speed during the first year (15 cm/s). Furthermore, the average velocity above 25 m is towards the west in the longer-term mean. This is consistent with a weakening of the boundary current core since the early 2000s.

Seasonal configuration

Nikolopoulos et al. (2009) demonstrated that, over the course of a year, the boundary current varies both in structure and strength. However, their conclusions were based on only one year of data. Here we use the full 6-year timeseries from the core of the jet to quantify the seasonal signal of the Beaufort shelfbreak current.

Climatological monthly mean volume, heat and freshwater transports

Using the proxy defined in section ‘Methods’, we constructed climatological monthly mean timeseries of volume transport (Sv), heat transport (J/s), and freshwater transport (m Sv) (Fig. 8). The data used for these monthly means are indicated in Table 2. One sees a pronounced seasonality dominated by the summer transport increase, which is associated with the appearance of the ACC. The months of June, July, August, and September account for approximately 85% of the yearly volume transport of the boundary current. During the remainder of the year the transport is significantly less, and is indistinguishable from zero during three of those months. November and May are both characterized by reversed flow to the west. Interestingly, these two months correspond to the two months of strongest upwelling activity on the Alaskan Beaufort slope (Pickart et al., 2013b). This suggests that wind forcing plays a significant role in the seasonality of the shelfbreak jet. To quantify this we also calculated the climatological monthly transports excluding time periods when the current was reversed (red dashed curves in Fig. 8). On average the boundary current reverses when winds exceed approximately 4 m/s from the east. In the absence of these strong easterly wind events there is still a clear seasonal strengthening of the current in summer, although the amplitude is reduced.

The seasonality of the heat and freshwater transports of the current is just as pronounced. In fact, nearly all of the heat transport occurs in the three months of July, August, and September. In the absence of strong easterly winds the heat flux is greater for every month of the year, with the biggest difference from July to December. Similar to the heat transport, most of the freshwater transport occurs in the months of July, August and September. However,

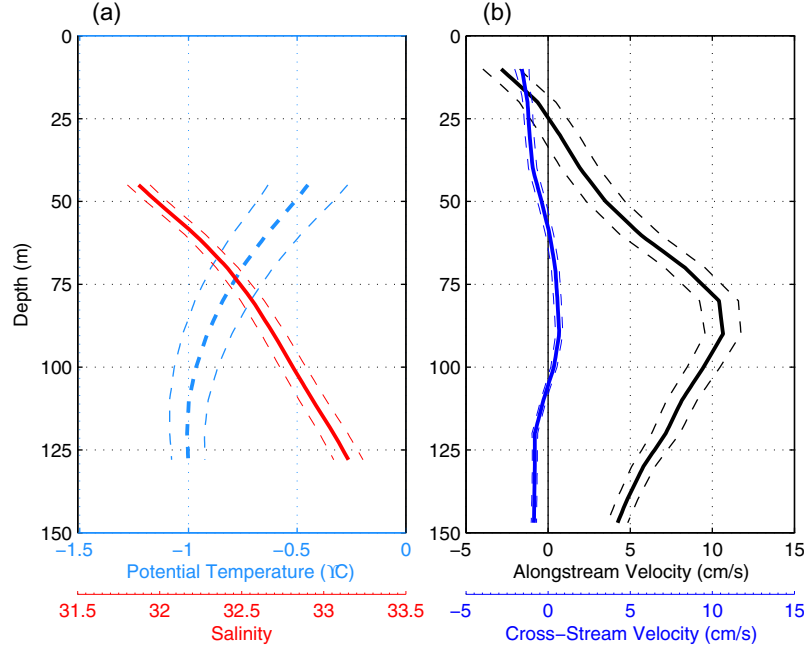


Fig. 7. Mean vertical profiles of (a) potential temperature and salinity, and (b) alongstream and cross-stream velocity over the six year-long deployments. Dashed lines represent the standard errors.

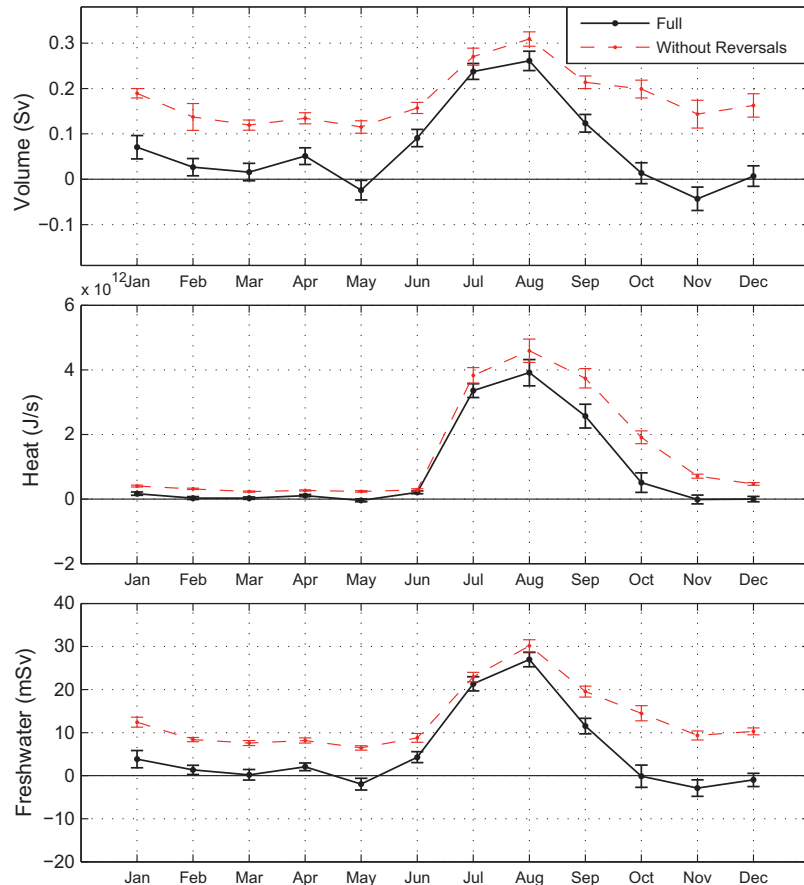


Fig. 8. Climatological monthly mean volume transport (Sv), heat transport (J/s) and freshwater transport (m Sv) of the Pacific water boundary current. Solid black lines represent the full transports, while red dashed lines represent time periods when the vertically averaged alongstream flow is not reversed. The standard errors are marked. (For interpretation of the references to colour in this figure legend, the reader is referred to the web version of this article.)

Table 2

Monthly inputs to the volume, heat and freshwater transport figures. X's denote both velocity and hydrographic data are available and O's represent only velocity data.

Year	January	February	March	April	May	June	July	August	September	October	November	December
2002	X						X	X	X	X	X	X
2003	X	X	X	X	X	X	X	X	X	X	X	X
2004	X	X	X	X	X	X	X	O				
2005							X	X	X	X	X	
2008							X	X	X	X	X	X
2009	X	X	X	X	X	X	X	X	X	X	X	X
2010	X	X	X	X	X	X	X	X	X	X	X	X
2011	X	X	X	X	X	O	O	O	O			

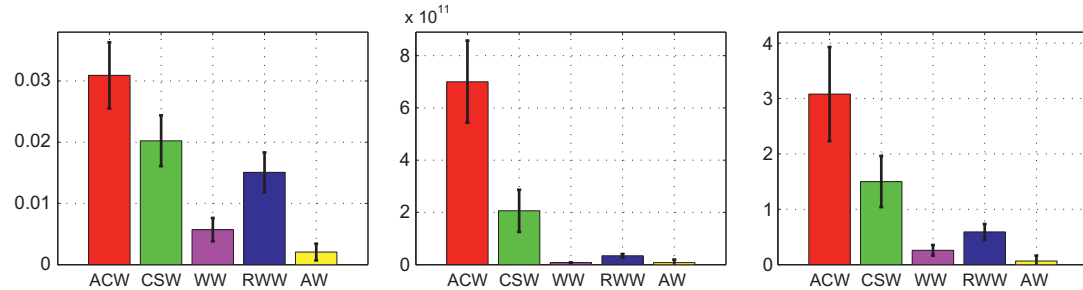


Fig. 9. Water mass contribution to the overall yearly (a) volume transport (Sv), (b) heat transport (J/s), and (c) freshwater transport (m Sv), including the standard errors.

unlike the heat flux, there is a small but significant freshwater flux in June.

Individual water mass transports

Strikingly, even though ACW is only present a few months of the year, in the mean it accounts for the majority of the volume transport (Fig. 9a). The next biggest contributor is the CSW, followed by the RWW, although their annual values are not statistically different from each other. Very little WW is transported to the east, likely due to the fact that wind forcing often reverses the shelfbreak jet when this water mass is present. Similarly, AW accounts for a very small fraction. Most of the heat transported by the shelfbreak jet past 152°W is associated with the warm ACW, with a smaller contribution from the CSW. The winter water masses RWW and WW advect a minimal amount of heat due to the cold temperatures of these waters. Finally, AW contributes very little to the heat transport due to the weak flow (or reversed flow) associated with upwelling events. As was true for heat flux, ACW and CSW are the dominant contributors to the freshwater transport in the shelfbreak jet, although CSW contributes a larger fraction than for the heat flux (Fig. 9c). Also, the winter waters transport a non-trivial amount of freshwater (in contrast to their heat flux, which is nearly zero).

Interannual variability

Next we consider the year-to-year variability of the Pacific water boundary current at 152°W. To assess this, we use the five full years of velocity data collected at the shelfbreak mooring site, where the year is defined as the period 1 August to 31 July. The reason for this definition is that it maximizes the data coverage (since the mooring is usually serviced in summer/fall). The years with complete records are 2002–2003, 2003–2004, 2008–2009, 2009–2010, 2010–2011 (2005–2006 has velocity coverage only in the fall since the ADCP failed prematurely).

Volume transport

Over the course of the last decade (2002–2011) the volume transport of the Pacific water boundary current has decreased dramatically (Fig. 10). During the first two deployments the transport was roughly 0.11–0.12 Sv, but five years later the transport had

dropped to the range of 0.021–0.041 Sv. This represents a reduction of nearly 80%. We note that this transport loss is qualitatively the same if we consider only the first three months of each year, in which case we can include an additional data point (2005–2006) whose value is in between the two clusters in Fig. 10. In 2009–2010 there was a slight “rebound” in transport to just over 0.04 Sv. In the analysis below we consider two regimes within the decade: the high transport period early in the decade and the low transport period later in the decade.

What water masses are associated with this pronounced reduction in transport? To assess this we considered the four years where there were corresponding hydrographic data over the same time period as the velocity data (see Table 2). The volume transports broken into the different water masses are shown in Fig. 11a. While there is considerable year-to-year variability for each water mass, there are clear trends. In particular, there is significantly more summer water transport (ACW and CSW) during the first two years than in the latter two years. In contrast, the changes in winter water transport (RWW and WW) are not as pronounced. Interestingly, there is no eastward flow of WW in two of the years (2003–2004 and 2009–2010), and the transport of CSW is particularly large in 2003–2004. Lastly, AW is either flowing westward (not represented in Fig. 11) or very weakly eastward throughout the study period.

Heat and freshwater transport

Since the largest decline in volume transport occurred for the two summer waters (ACW and CSW), not surprisingly there is also a substantial drop in the heat and freshwater transport of these two water masses from 2002 to 2011 (Fig. 11b and c). However, a reduction in heat content of the ACW and CSW over this time period (not shown) makes the decrease in heat flux between the early and later years even more dramatic. Individually, the ACW heat flux declined by 90%, while the CSW heat flux decreased by 80%. There is a similar discrepancy between the early years and later years for the freshwater transport. While the freshwater transport is dominated by the ACW and CSW in the early years, there is hardly any summer water freshwater flux in 2008–2009, and in the following year the RWW contributes to the freshwater flux as much as the two summer water masses. Woodgate et al. (2012) show that there has been an increase in the volume and

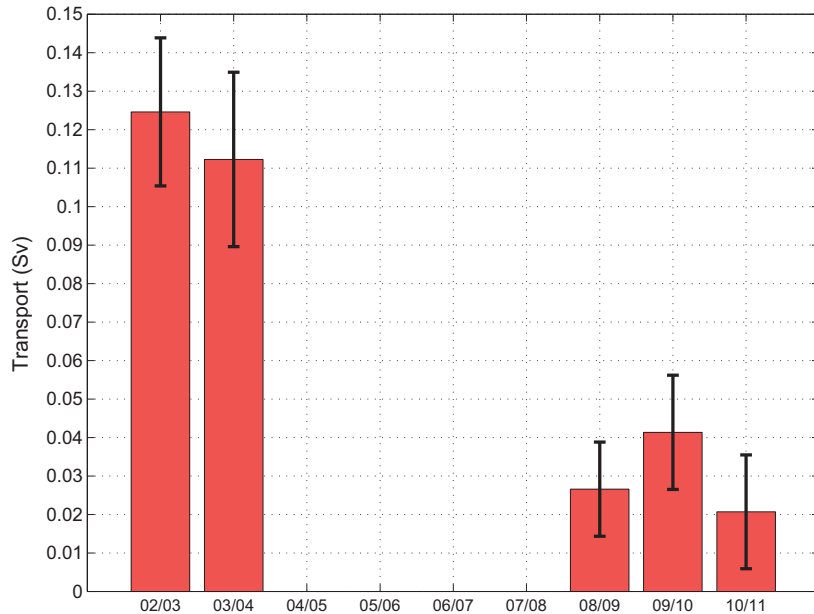


Fig. 10. Yearly volume transport (Sv) of boundary current measured by the shelfbreak mooring, including the standard error. Years are defined from 01 August to 31 July.

heat flux through Bering Strait over the past decade, suggesting that the changes in the transport of the shelfbreak jet in the Alaskan Beaufort Sea presented here are not remotely driven. This, together with the noticeable change in seasonality of the flow in the absence of easterly wind events (Fig. 8a), suggests that wind forcing is key. We now investigate the role of atmospheric forcing in an attempt to explain the signals seen in Fig. 10.

Nature of the atmospheric circulation in the Pacific Arctic

Mean circulation

Local winds on the Beaufort slope are, to first order, driven by two atmospheric centers of action: the Beaufort High (BH) and the Aleutian Low (AL). The BH appears as an isolated feature north of Alaska or as a region of high pressure that extends from the East Siberian Sea to the Beaufort Sea. The BH shows up clearly in the decade-long (2002–2011) mean of sea-level pressure (SLP) using the NARR re-analysis fields (Fig. 12a). The AL is the integrated signal due to low pressure systems that traverse from west to east along the North Pacific storm track (Wilson and Overland, 1986; Pickart et al., 2009b). The systems tend to intensify in the region of the Aleutian Island chain. The AL is evident as well in the decade-long mean of Fig. 12a as an area of low pressure centered over the island chain extending into the Gulf of Alaska. Together, these two large-scale atmospheric features result in a SLP gradient that promotes easterly winds in the Alaskan Beaufort Sea. Indeed, the Pt. Barrow weather station data indicate that the most frequent and most intense winds in the region are out of the east to northeast.

Seasonal circulation

Seasonally, the two centers of action vary in both strength and location. During autumn and winter the AL deepens due to the combined effect of more frequent and stronger storms (Fig. 12b). Pickart et al. (2009a) demonstrated that some of these storms are broad enough in extent and track far enough to the north to trigger upwelling events on the north slope of Alaska. These Pacific-born storms occur much less frequently during spring and summer, and, as such, the AL is almost indistinguishable during this time period (Fig. 12c). The BH also has marked seasonal variability.

In the fall and winter, when the AL is intensified, the BH is part of a ridge of high pressure extending from the East Siberian Sea to the Beaufort Sea (Fig. 12b). Serreze and Barrett (2011) demonstrate that the Siberian High and the Yukon High influence the structure of the BH this time of year. During the spring and summer the BH is more of a distinct feature that is confined to the Beaufort Sea region (Fig. 12c).

In light of the seasonality of the two centers of action, it is not surprising that the winds measured at the Pt. Barrow weather station vary throughout the year. Following Pickart et al. (2013b) we computed the climatological monthly mean alongcoast wind for the 70-year Pt. Barrow data set. In each month the mean winds are out of the east, with two seasonal peaks. The first occurs during the October/November timeframe, and is a result of the enhanced SLP gradient between the Beaufort High and the deep Aleutian Low. The second peak occurs in May when there is no strong signature of the AL. However, when storms develop that time of year they have a more northward track and thus amplify winds on the north slope of Alaska (Pickart et al., 2013b). Climatologically, the weakest easterly winds occur during the summer, specifically in July and August when the Beaufort High is well developed and situated over the southern Beaufort Sea and western Canadian Archipelago (Moore, 2012).

Interannual variability

In light of the results of the previous section, where it was demonstrated that most of the interannual change in transport of the Beaufort shelfbreak jet has occurred during the summer months, we focus on the year-to-year atmospheric variability for the months of June, July and August (JJA). While the NARR JJA fields indicate substantial year-to-year variability, the overall trend through the decade was a strengthening of the summer BH in this part of the western Arctic. In general the AL is weak during the summer months, and this decade was no exception. However, the AL did become more pronounced over the 10-year period; in particular, while only traces of the AL were apparent in the first part of the decade (2003, 2005, 2006), it became much more prevalent during the last four years (2008–2011). The Pt. Barrow weather station data reveal that the JJA alongcoast winds strengthened by 5 m/s over this period. We now investigate the consequences of these interannual

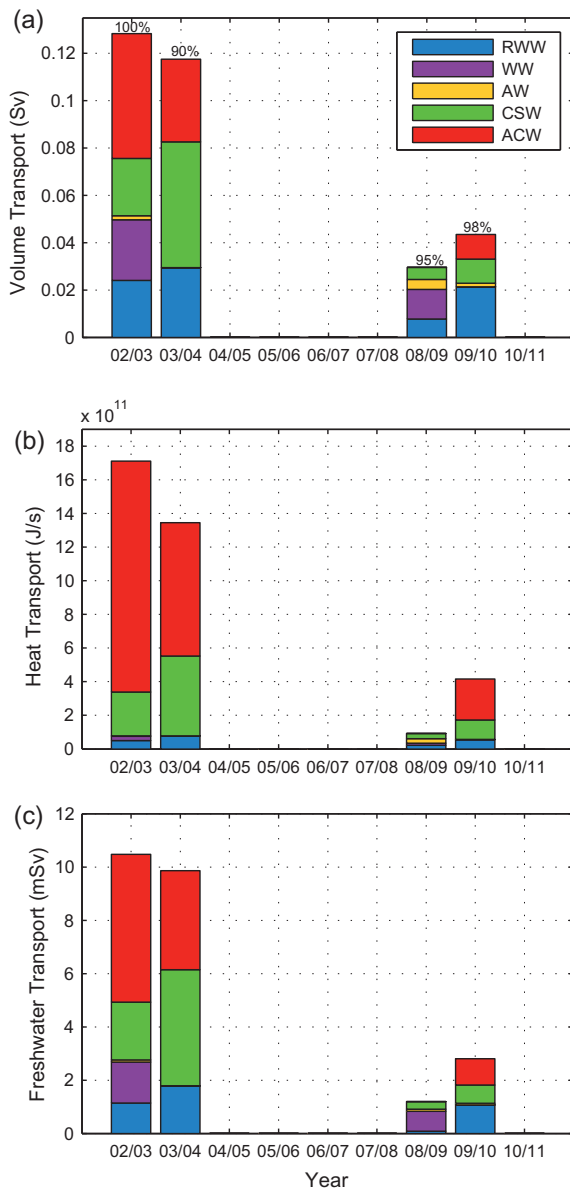


Fig. 11. Yearly (a) volume transport (Sv), (b) heat transport (J/s), and (c) freshwater transport (mSv) of the boundary current measured by the shelfbreak mooring broken into the five water masses. Years are defined from 1 August to 31 July. The percentages at the top of each bar indicates the amount of the year that both velocity and hydrographic properties were measured simultaneously.

changes in atmospheric forcing, as well as variation in other physical drivers, on the Beaufort shelfbreak jet.

Physical drivers of the Pacific Arctic boundary current

Atmospheric forcing

Previous studies have shown that local wind forcing influences the strength of the shelfbreak jet in the Alaskan Beaufort Sea. In particular, easterly winds can diminish the alongstream flow and readily reverse it, which leads to upwelling and significant shelf-basin exchange (e.g. Nikolopoulos et al., 2009; Pickart et al., 2009a, 2013a). Although not as common, westerly winds can accelerate the current to the east and drive downwelling. The long time-series of transport in this study allows us to more robustly explore the relationship between the atmospheric forcing and boundary current strength.

Relationship between summer transport and wind speed

When considering the five summers for which complete transport data are available (2003, 2004, 2009, 2010, 2011), the strong relationship between local wind speed and current transport is evident (Fig. 13). Summer 2003 is characterized by very weak easterly winds along the Beaufort slope, which are not significantly different than zero. Not surprisingly, the transport during that summer is the largest of all five years. Easterly wind speeds increase in 2004 and the current transport diminishes slightly. In the latter part of the decade the easterly winds increased significantly, in concert with the diminished boundary current transport. As pointed out earlier, the shelfbreak jet “rebounds” in summer 2010 (~ 0.15 Sv), which is associated with a corresponding slackening of the easterly winds.

Sea level pressure gradient

The strong correspondence between summertime averaged local wind speed and boundary current transport in Fig. 13 motivates us to clarify more carefully the nature of the wind. As noted in section ‘Nature of the atmospheric circulation in the Pacific Arctic’, it is the gradient in SLP between the two centers of action, the BH and AL, that primarily drives the winds along the Beaufort slope. One might wonder to what degree each center of action is contributing to the interannual variability in SLP. It would be reasonable to assume that it is primarily the BH because the summertime signature of the AL is so much weaker in comparison to the fall and winter. To answer this question we calculated the extent to which the BH and AL individually influence the SLP gradient each year as follows.

For each summer, the central locations of the BH and AL were identified in the NARR fields based on maximum and minimum regions of SLP respectively (pressure values over land were not considered). Summer 2002 is an exceptional case in that there is no signature of the AL in the Bering Sea or Gulf of Alaska. Consequently, for that year the AL was chosen to be in the same location as the decadal mean AL position for JJA. To isolate the effect of the BH, we assumed that the AL has a constant central SLP of 1010.8 mb and is positioned 2300 km away from the center of the BH (based on the decadal mean SLP for JJA) and then used the measured variation in central SLP of the BH. Analogously, to isolate the role of the AL we assumed that the BH has a constant central SLP of 1015.2 mb and is similarly positioned 2300 km away from the center of the AL (again based on the decade mean SLP for JJA). Finally, we estimated the actual SLP gradient by taking into account the variation in the magnitude of both centers of action as well as the distance between them. (We note that for the above mentioned calculation, the BH-only and AL-only SLP gradients do not sum to the actual SLP gradient for this time period.)

Over the decade, both the BH-only SLP gradient and the AL-only SLP gradient increased as a result of the strengthening and deepening of the two centers of action, respectively (Fig. 14a). Interestingly, one sees that the trend in the AL-only value is more in line with the actual SLP gradient trend (Fig. 14a), accounting for the majority of the decadal change. Although not considered in this study, there is indication that a trend towards lower pressures over Alaska is also likely contributing to the increasing gradient. The situation is reversed, however, with regard to the year-to-year fluctuations. The detrended SLP gradient timeseries shows a much higher correlation between the actual SLP value and the BH-only value (Fig. 14b). Hence, while the decadal trend in SLP gradient is influenced most strongly by the AL, the year-to-year variability in SLP gradient is driven principally by the BH.

Reconstructing the shelfbreak current observations

We now investigate the degree to which the year-to-year change in transport can be predicted based solely on the winds.

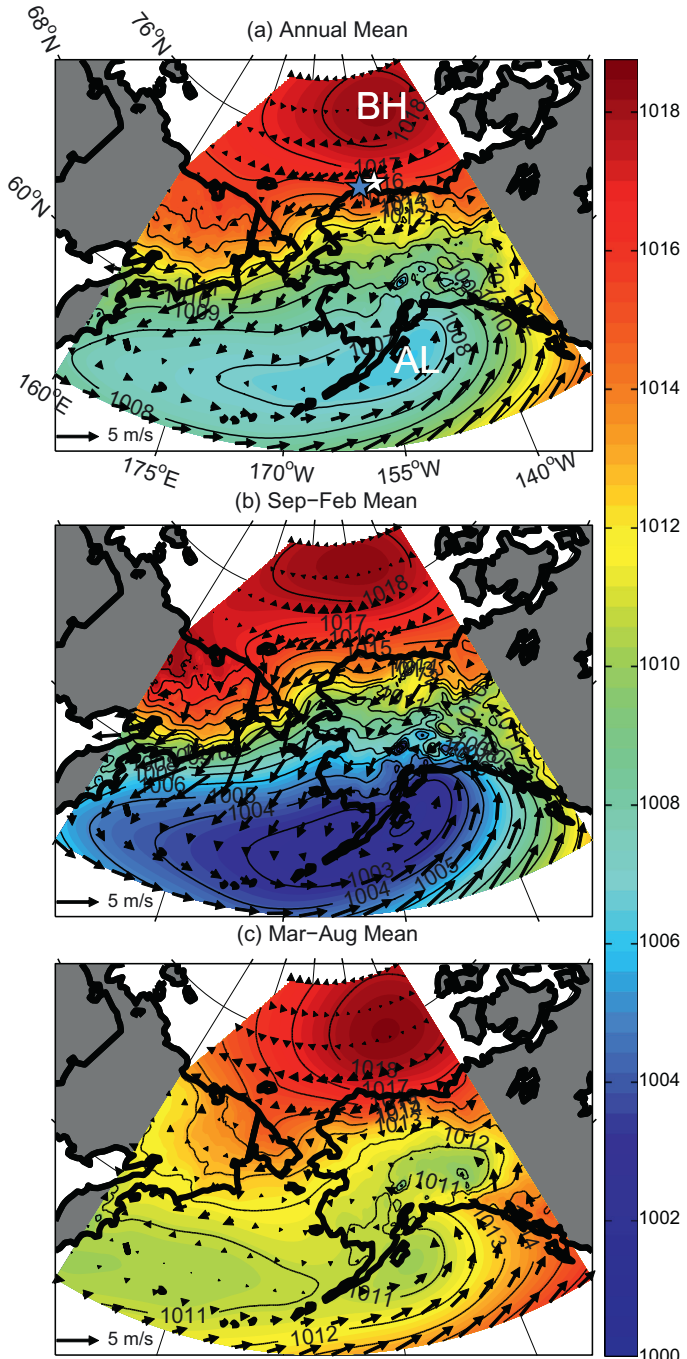


Fig. 12. (a) Mean sea-level pressure (contours and shading, mb) for the period 2002–2011. (a) Year-long mean; (b) September–February mean; and (c) March–August mean. Overlaid are 10 m wind vectors (m/s). The Beaufort High (BH) and Aleutian Low (AL) are labeled. The white star indicates the location of the shelfbreak mooring and the blue star indicates the location of the Pt. Barrow weather station. (For interpretation of the references to colour in this figure legend, the reader is referred to the web version of this article.)

To do this we regressed the daily mean alongcoast wind speed measured by the Pt. Barrow weather station versus the daily mean transport of the boundary current for the combined time period of all five summers. In the absence of wind, the Pacific water boundary current transports 0.27 ± 0.08 Sv to the east, which is about one-third of the long-term transport through Bering Strait (Woodgate et al., 2005c). Overall, the predicted summer transport compares well to the measured value for the five years of mooring data (Fig. 15). One sees that the trend of decreasing transport through the decade is nicely captured, and the qualitative year-to-year variability is reflected in the predicted value as well.

There are, however, significant discrepancies between the transport predicted by the local winds alone versus the measured transport. For example, the reconstructed transport systematically underestimates the high transport in the early part of the decade (2003 and 2004), and overestimates the low transport in the later part of the decade (2009, 2010 and 2011). The primary reason for this is the interannual variability in the strength of the undisturbed current during summer. This was demonstrated by performing individual regressions for each of the five summers and tabulating the y -intercept each year. This reveals that the undisturbed flow along the Beaufort slope was greater in the early part of the decade,

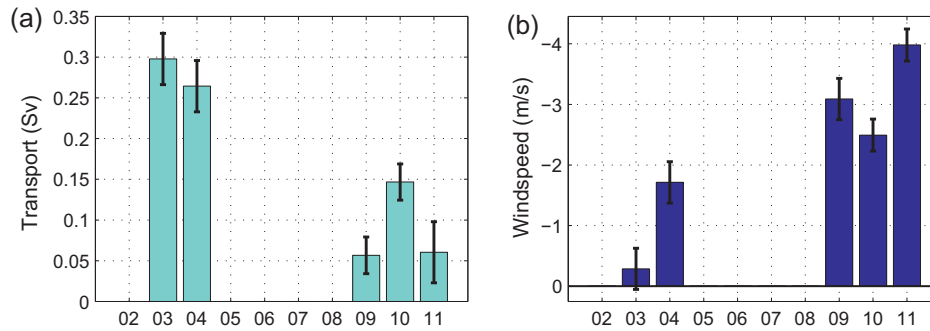


Fig. 13. (a) Mean volume transport (Sv) of boundary current including the standard error for June, July and August. (b) Mean alongcoast wind speed (105°T) including the standard error for June, July and August.

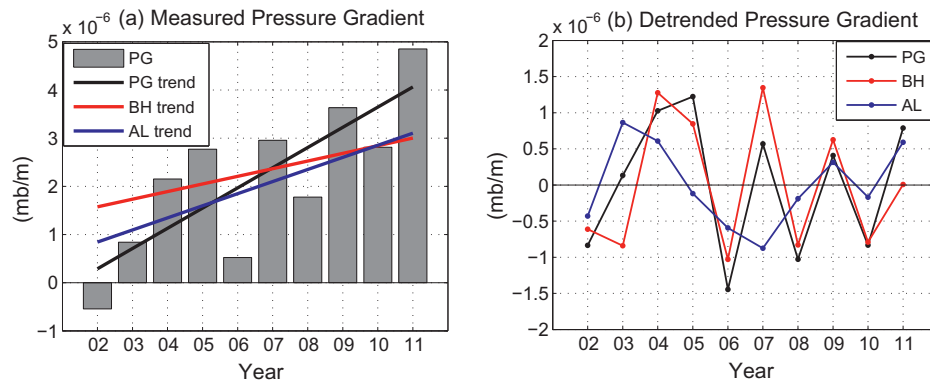


Fig. 14. (a) Pressure gradient determined from mean SLP for June, July August over the decade 2002–2011 (gray bars), including trend line (black). Also shown are the trend lines for the pressure gradients when considering the BH only (red) and AL only (blue). (b) Detrended SLP gradient over the Beaufort slope. The black line is the full pressure gradient, the red line is the BH only pressure gradient, and the blue line is the AL only pressure gradient. (For interpretation of the references to color in this figure legend, the reader is referred to the web version of this article.)

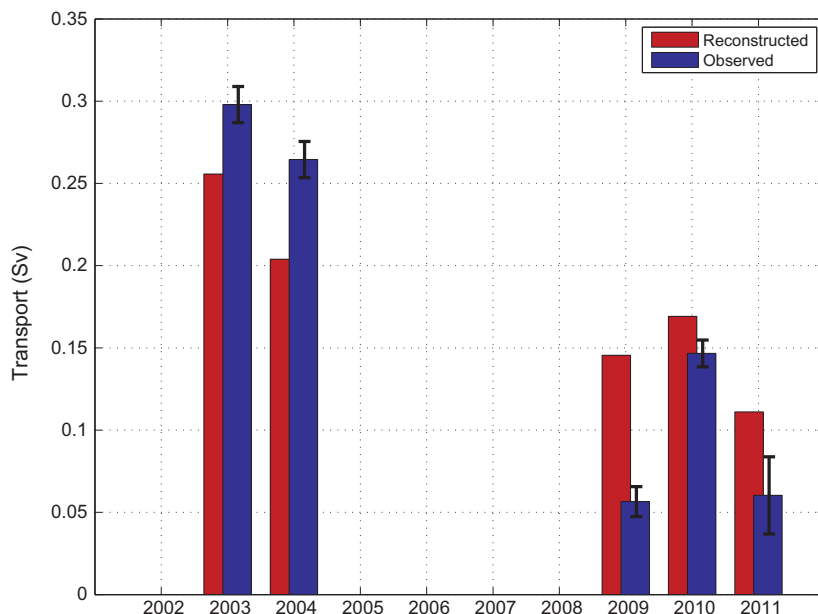


Fig. 15. Mean measured volume transport (Sv) of boundary current including the standard error for June, July and August (blue) and the reconstructed mean volume transport (Sv) for June, July and August based on the relationship of current transport and wind speed (red). (For interpretation of the references to color in this figure legend, the reader is referred to the web version of this article.)

and decreased to smaller values in the later years (gray bars in Fig. 16).

Upstream influences

The fact that the undisturbed flow of the Beaufort shelfbreak jet can change from year-to-year should not come as a surprise. [Woodgate et al. \(2012\)](#) recently showed that the pressure head contribution to the Bering Strait inflow varies on interannual time scales. They demonstrated that in recent years this contribution has increased, and is in fact the primary reason for the enhancement in Bering Strait transport. It is natural then to wonder if the transport of the undisturbed boundary current on the Beaufort slope presented here has varied in concert to that in Bering Strait over the study period.

To investigate this it is necessary to consider only the flow of summer water through Bering Strait ([Woodgate et al.'s, 2012](#) analysis considered the full year). Consequently, we used the eastern-most mooring in the strait, mooring A4, which captures the signal of the near-shore ACC ([Woodgate and Agaard, 2005](#)). Performing the analogous summertime regressions (using the NARR winds), we estimated the undisturbed transport of Pacific summer water through Bering Strait for each of the five years, which is compared to that for the Beaufort shelfbreak jet in Fig. 16. One sees that during the early part of the decade the agreement is very good, and in 2010 the values are again fairly close (especially in light of the error bars). Recall that 2010 was the rebound year. However, in 2009 and 2011 the undisturbed flow on the Beaufort slope is significantly smaller than that through Bering Strait. We suspect the reason that the undisturbed values at the two sites may not always track each other is because of their large geographical separation, and, as such, the undisturbed flow on the Beaufort slope may not always reflect undisturbed flow along the upstream pathway from Bering Strait to Barrow Canyon.

To test this notion we compared the alongcoast winds on the north slope of Alaska to those in the Chukchi Sea (along the west coast of Alaska) using the NARR data. The Beaufort domain extends from Pt. Barrow eastward to 148°W, while the Chukchi domain extends northward from Bering Strait to Pt. Barrow. We found that in 2003, 2004, and 2010 (i.e. the years when the undisturbed

transports were in close agreement) the winds were significantly correlated between the two domains, while in 2009 and 2011 (when the undisturbed transports differed) there was no correlation. Conceptually this makes sense in that when the winds are correlated all along the pathway from Bering Strait to the Beaufort slope, the transports would be similar at the two locations when the wind abates. In contrast, for summers when the wind in the Chukchi Sea varies independently from that on the Beaufort slope, the flow entering the Beaufort domain during times of weak local winds was likely subject to wind forcing during some part of its transit through the Chukchi Sea. We note that in 2009 and 2011 – when the undisturbed Beaufort slope transport was weaker than that in Bering Strait – the winds in the Chukchi domain were enhanced out of the north and opposed the northward flow of Pacific water.

Sea ice

In light of the significant changes in sea ice cover in this part of the Arctic Ocean, it is of interest to determine if this has had any effect on the transport of the Pacific water boundary current. The water column response to easterly winds over the Beaufort slope is most pronounced in the presence of a partial ice cover ([Schulze and Pickart, 2012](#)). This is due to an increase in stress imparted to the ocean via the freely moving ice keels. Under these conditions the shelfbreak jet is readily reversed and attains its highest speeds to the west. In contrast, the water column has the weakest response when there is complete ice cover. Finally, there is a more moderate response when the area is ice free.

To investigate this we considered the average sea ice concentration in a 70 km (zonal) by 70 km (meridional) box surrounding the mooring. It was found that the concentration was, for the most part, similar for four out of the five years (2003, 2004, 2009, and 2011). In these years, complete ice cover existed during June, then the concentration rapidly lessened during July and open water occurred near the beginning of August. The seasonal evolution of the ice field was noticeably different in 2010. During that year, full ice conditions persisted until late July, and partial ice was present over the first half of August. In addition, August 2010 was characterized by particularly strong easterly winds. As such, one might have expected the boundary current to be considerably weaker

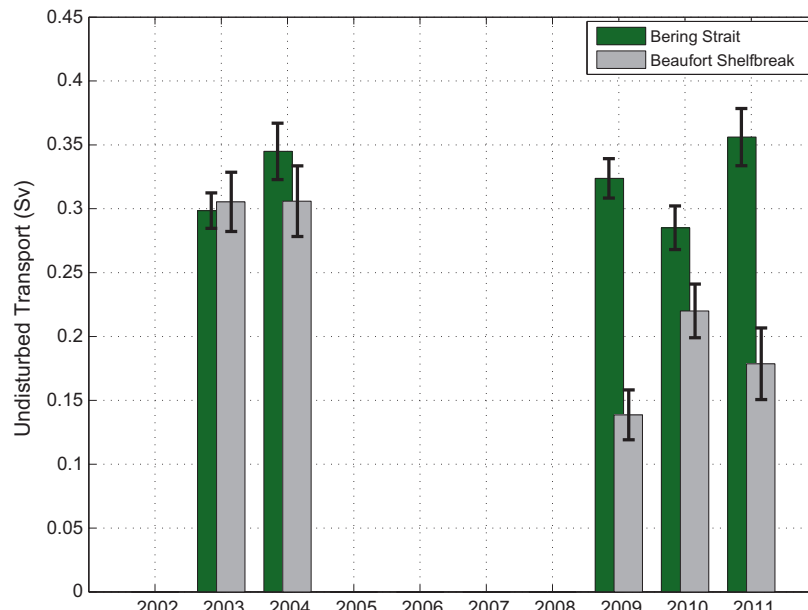


Fig. 16. Undisturbed transport (Sv) of the Beaufort shelfbreak jet (gray) and the Alaskan Coastal Current at Bering Strait (green) for each summer. (For interpretation of the references to color in this figure legend, the reader is referred to the web version of this article.)

that month compared to August of the other years. However, this was not the case. Overall, we found no compelling evidence that ice concentration affected the transport of the boundary current during the time period of the study.

Discussion: implications of a diminished Pacific water boundary current

Between 2001 and 2011 there has been a 50% increase in the volume transport through Bering Strait, and, correspondingly, the amount of heat and freshwater entering the Arctic from the Pacific has increased as well (Woodgate et al., 2012). Over this same time period, however, the transport of the Pacific water boundary current in the Beaufort Sea has decreased by more than 80%, with the most dramatic changes occurring during the summer months associated with the two summer water masses – Alaskan Coastal Water (ACW) and Chukchi Summer Water (CSW). We have shown that the atmospheric forcing in summer has been the main driver of this change; in particular, an intensification of the Beaufort High (BH) and a deepening of the Aleutian Low (AL). Together, these centers of action have led to enhanced easterly winds in the Alaskan Beaufort Sea that have opposed the boundary current and made it difficult for Pacific water to progress eastward along the Beaufort shelfbreak in recent years.

Previous modeling studies have addressed the impact of the wind on the pathways of Pacific water in the western Arctic. Using a barotropic model, Winsor and Chapman (2004) illustrated that strong northeasterly and easterly winds reverse the flow along the Beaufort shelfbreak. Under this wind regime, the Pacific water exits the Chukchi Sea in a more northward direction and enters the Canada Basin. Watanabe (2011) used a numerical model in combination with satellite data to examine the shelf-basin exchange in the western Arctic region. They argued that, during summer 2007, the shelfbreak jet was nonexistent due to the enhanced easterly winds, and hence no Pacific Water entered the Alaskan Beaufort Sea. Instead, the majority of the Pacific water veered westward from Barrow Canyon and much of it entered the Canada Basin as a result of offshore Ekman transport. In terms of atmospheric forcing, summer 2007 is similar to the final three years of our study period (2009, 2010 and 2011) in that there are strong easterly winds along the Beaufort slope. While the Beaufort shelfbreak jet was present in those years, its transport was largely diminished. This raises the question as to the pathways of Pacific summer water in the later part of the decade and what the implications are for the western Arctic system.

Summer heat and freshwater transports

In Section ‘The Pacific water shelfbreak current’ we computed the heat and freshwater fluxes of the Beaufort shelfbreak jet for each year, where the year was defined as the period from 1 August to 31 July (this definition was used to maximize the data coverage). We now consider the subset of months June, July, August, and September to capture the full signal of summer water in a given calendar year (the previous definition split the summer into two different years). Considering this timeframe gives three full summer water seasons: 2003, 2009 and 2010. We find that the cumulative amount of heat advected past the mooring in summer 2003 had the potential to melt up to 168,000 km² of 1 m thick ice, while the average value for 2009–2010 was 51,000 km². This difference (more than 100,000 km²) represents an area roughly one-third the size of the Beaufort shelf.³ With regard to the freshwater,

fully developed boundary current in summer 2003 transported a total of 300 km³ of freshwater past the mooring site, while the average of the latter two years was roughly 70 km³. This discrepancy (230 km³) is comparable to the average year-to-year change in the freshwater content of the Beaufort Gyre during the last decade (175 km³, see Pickart et al., 2013a). These results demonstrate that a substantial amount of heat and freshwater – enough to influence ice melt as well as the freshwater accumulation in the basin – has been diverted away from the Beaufort slope in recent years and has gone somewhere else. The question is, where?

Sea ice in the Pacific Arctic

A number of studies in recent years have addressed the role of Pacific water on sea ice melt in the western Arctic Ocean. Shimada et al. (2006) argues that there is a recently developed feedback loop where the combination of reduced ice stress and anticyclonic wind forcing (associated with the BH) direct the warm Pacific summer water into the Canada basin causing significant changes in sea ice cover. Using an ice-ocean numerical model, Steele et al. (2010) investigated the different causes of sea ice melt in the Pacific sector of the Arctic, defined as the region encompassing the Chukchi, Beaufort, Laptev and East Siberian Seas, as well as the adjacent deep basin. They concluded that basal melt of sea ice (via the ocean) contributes roughly two-thirds of the total volume melt, but is geographically constrained to the marginal ice zone. The surface melt (via the atmosphere) contributes one-third of volume melt and occurs over a much broader area of the ice pack. Steele et al. (2010) further considered the portion of basal melt due to local atmospheric heating of the water (adjacent to the ice) versus that due to remote advection by ocean currents (i.e. the Pacific water). They concluded that the dynamical oceanic contribution accounts for about two-thirds of the basal melt. Therefore, it is clear that Pacific water inflow plays a significant role in melting sea ice in the Pacific sector.

Distributions of sea ice melt and formation

Ice melt. Returning to the five study years considered in the previous section, we present the late September sea ice concentration fields for 2003, 2004, 2009, 2010 and 2011 in Fig. 17. These fields reflect the cumulative effects over the summer of both atmosphere-forced and ocean-induced sea ice melt. One sees that there was a significant difference in the extent and character of the ice melt in the later years (2009, 2010, 2011) versus the earlier years (2003 and 2004). In particular, the ice edge was farther offshore in the Canada Basin in the later years. We consider the amount of ice in the region marked in Fig. 17 north of the Chukchi and Beaufort shelves. This area was chosen because it captures the area where the largest interannual changes occur. Furthermore, this area encompasses a likely destination for Pacific water if it is not channeled eastward into the Beaufort shelfbreak jet, but instead gets fluxed seaward into the interior basin. In 2003 and 2004 there was approximately 93,984 km² and 123,420 km² of sea ice, respectively, within the measurement box. This is to be contrasted to the later years when there was 37,443 km², 34,024 km², and 27,747 km² in 2009, 2010, and 2011, respectively. This amounts to a difference of approximately 76,000 km² between the early and later years. Based on the calculations above, the discrepancy in the cumulative amount of heat fluxed past the mooring site for the early years versus the later years (~100,000 km²) is more than enough to account for the difference in ice melt within the measurement box (~76,000 km²) over this time period.

Freeze-up. It was also suggested by Steele et al. (2010) that, rather than melting the pack ice, Pacific summer water might delay ice formation in early fall in the region north of the Chukchi Sea. To

³ We note that this is an upper limit, as it assumes that there is no heat loss to the atmosphere and that subduction does not occur.

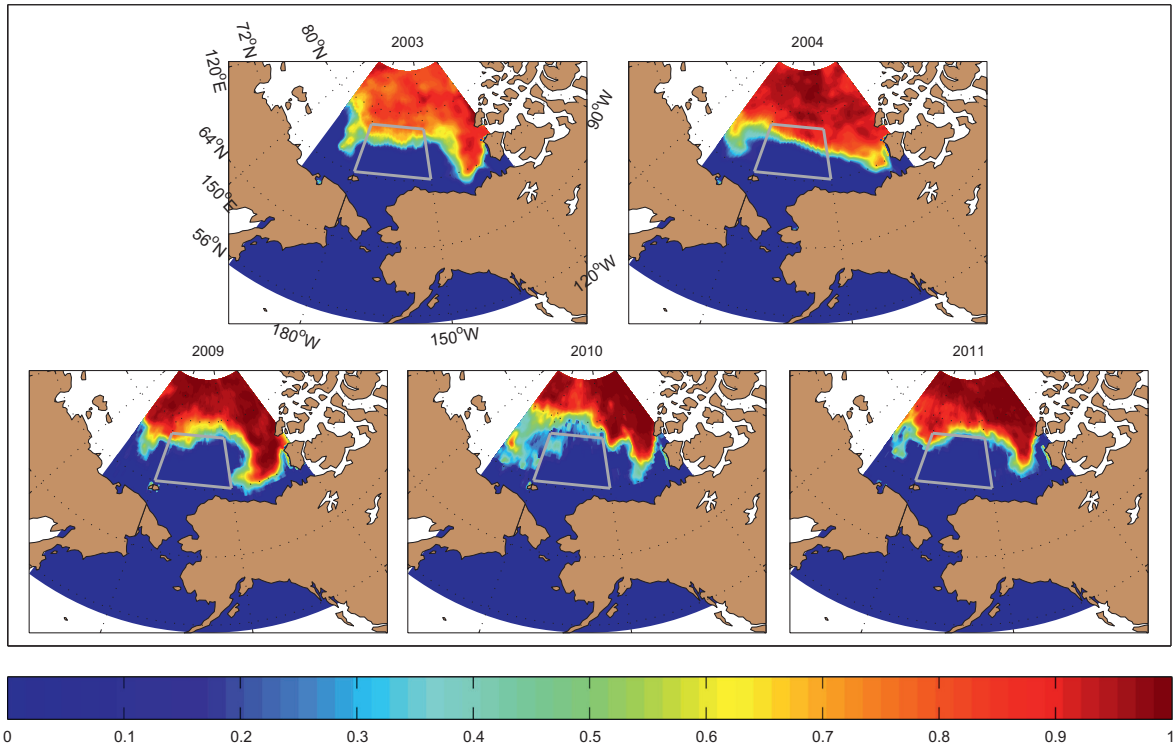


Fig. 17. Mean sea ice concentration in the Pacific sector of the Arctic Ocean from 15 September to 31 September. The gray box is the region used to determine differences in ice melt (see text).

assess this, we consider the sea ice concentration fields for the time period 1 October to 15 November. This 6-week period is chosen because, for the years considered, freeze-up generally begins by early October, and mid-November is when the measurement box is completely re-covered with sea ice in 2003. The satellite data set ends on 4 October 2011 and therefore we do not consider that year. We find that 2003 and 2004 are quite similar; in particular, there is a substantial re-freezing from October into November. However, in 2009 and 2010 there was still a significant area of open water within the measurement box. The difference in ice extent within the measurement box between the early years and late years is approximately 50,000 km². Again, the amount of heat that did not enter the Beaufort shelfbreak jet could readily account for this change.

Pacific water exiting the northeast Chukchi sea

The above conclusions assumed that all of the heat not entering the Beaufort shelfbreak jet east of Pt. Barrow was available either to melt ice in the basin or delay the onset of freeze up. However, it is unclear how much of the Pacific summer water actually made it to Barrow canyon in the latter part of the decade, and, if it did, what the fate of the water was that exited the canyon.

Using a combination of mooring and satellite data, Okkonen et al. (2009) investigated how different wind regimes impact the summertime flow of Pacific water (i.e. the ACC) within Barrow Canyon. They showed that when the winds are easterly, southeasterly, or southwesterly, the ACC flows northward along the eastern flank of the canyon. However, in the former two cases, if the wind is strong enough, it drives westward flow on the Beaufort shelf that tends to oppose the penetration of the warm summer water to the east. The other case that Okkonen et al. (2009) considered was northeasterly winds. These are approximately aligned with Barrow Canyon, and, consequently, the flow of the ACC on the eastern flank is reversed. In this scenario it is unclear how much warm Pacific water actually enters the canyon; Okkonen et al. (2009) suggest

that some portion of the ACC gets diverted to the western side of the canyon.

Due to the strong easterly/northeasterly winds during the latter three summers in our study period, it is possible that a portion of the ACC volume and heat flux did not make it to Barrow Canyon, but instead was redirected onto the Chukchi shelf. In that case it would not be accurate to presume that all of the water not entering the Beaufort shelfbreak jet is fluxed into the Canada Basin (and hence available to melt ice there). This is now addressed using ancillary data from 2011.

Evidence from a moored array

An array of moorings was deployed at the head of the canyon during summer 2011 as part of a study funded by the Bureau of Ocean and Energy Management to investigate the circulation in the northeast Chukchi Sea. One mooring in particular, BC2, was located in the center of the ACC in 50 m of water and included an upward-facing ADCP to measure velocity through the water column. A Microcat located near the bottom of the mooring (48 m) measured temperature and salinity. Unfortunately, the CMP on the Beaufort shelfbreak mooring at 152°W failed in late-May that year. However, the Microcat at 35 m provides an effective proxy for the temperature of the summer water in the shelfbreak jet. In order to carry out a consistent comparison of the heat flux at the two sites (Barrow Canyon and 152°W), we considered only the velocity measurements at 45 m on each mooring. Because the hydrographic data at 152°W were collected 13 m higher in the water column than in Barrow Canyon, we used the temperature gradient (calculated from previous years) to adjust the temperature at the shelfbreak site. Based on earlier shipboard hydrographic/velocity measurements from the SBI program, along with the 2011 mooring array data, it is estimated that the ACC has a width of 20 km at the head of Barrow Canyon (recall that the width of the Beaufort shelfbreak jet is 16–18 km). We consider the full time period that summer water was present at each location in 2011. In Barrow Canyon the warm water first appeared in early-June

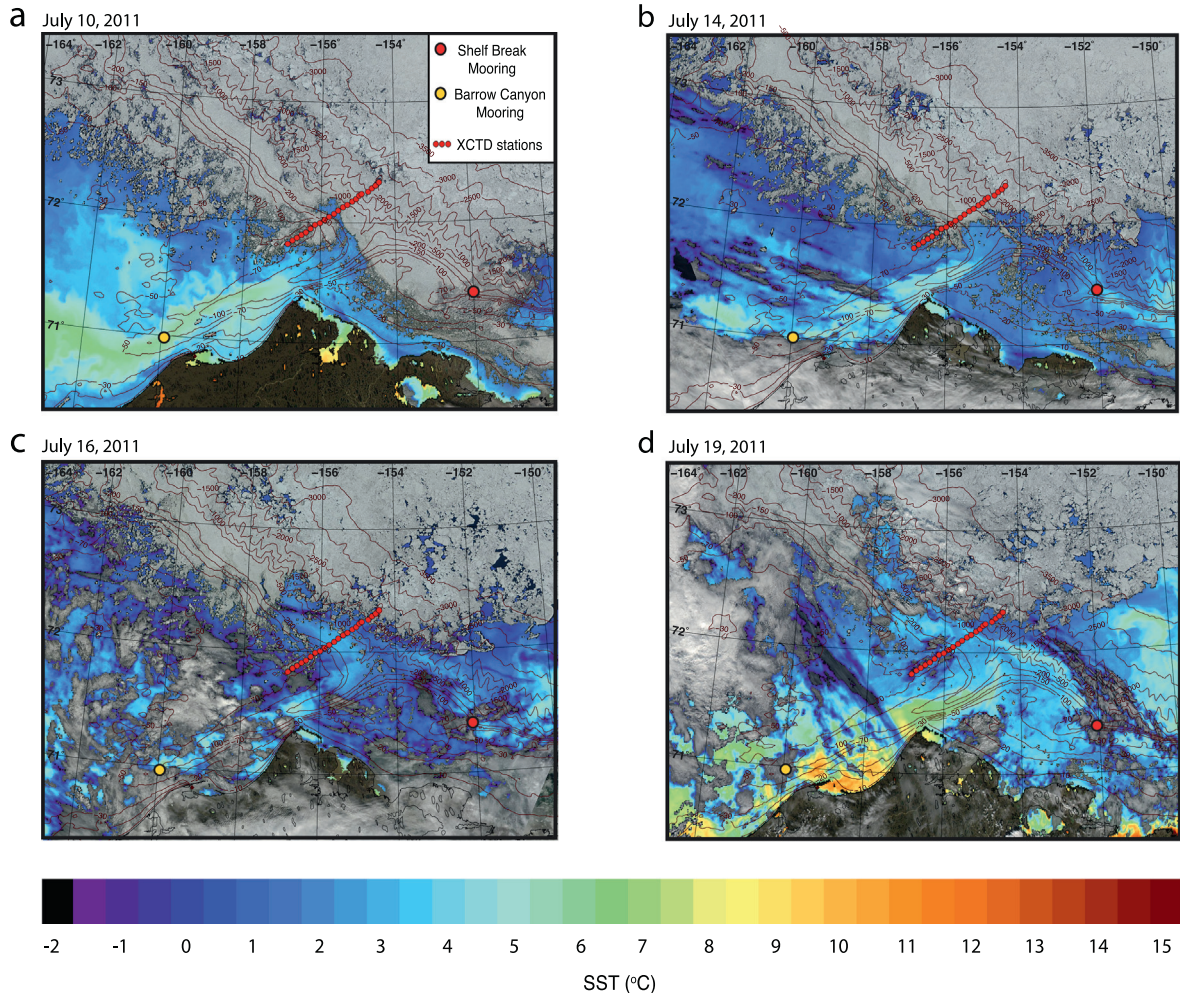


Fig. 18. Satellite images of study region showing sea surface temperature and visible imagery for (a) 10 July 2011, (b) 14 July 2011, (c) 16 July 2011, and (d) 19 July 2011. The Beaufort shelfbreak mooring is indicated by the red circle and the Barrow Canyon mooring is indicated by the yellow circle. The locations of the USCGC Healy XCTD stations are indicated by the line of red circles. (For interpretation of the references to color in this figure legend, the reader is referred to the web version of this article.)

and persisted until mid-October, while at 152°W for the Beaufort shelfbreak jet it was present from early-July to mid-October.

Our calculation reveals that significantly more heat was fluxed northward through the head of Barrow Canyon than was fluxed eastward past 152°W in the Beaufort shelfbreak jet, $2.02e + 12 \pm 2.58e + 11$ J/s versus $6.28e + 11 \pm 2.07 + 11$ J/s. The difference is enough to melt roughly $52,000 \text{ km}^2$ of 1-m thick sea ice, with a range of $35,000 \text{ km}^2$ – $70,000 \text{ km}^2$ when considering the error bars. Even with this uncertainty it is clear that a considerable amount of the heat reaching Barrow Canyon in summer 2011 did not enter the Beaufort shelfbreak jet – enough to account for much or all of the decrease in sea ice within the measurement box of Fig. 17 in the latter years of our study period ($76,000 \text{ km}^2$). But the question remains, where did the heat go? One possibility is that, following the ideas in Okkonen et al. (2009), the ACC was diverted to the western side of Barrow Canyon and exited the canyon as a westward-flowing jet along the edge of the Chukchi shelf. Another possibility is that the summer water was fluxed directly northward into the basin via turbulent processes such as eddy formation. A third possibility is that a jet of warm water emanated from the canyon which was not trapped to the shelf edge. At this point it is impossible to say which of these scenarios is most likely, or if all of them can happen over the course of a summer. However, shipboard and satellite data obtained in summer 2011 during an

easterly wind event demonstrates that the third scenario is a viable mechanism for exporting heat out of Barrow Canyon into the Canada Basin.

Evidence from satellite and shipboard data

During July 2011 two prolonged easterly wind events took place in the vicinity of Barrow Canyon and the Alaskan Beaufort Sea. During the first event, which lasted more than two weeks and had peak easterly winds over 10 m/s, the USCGC *Healy* occupied a XCTD/velocity section to the west of the canyon mouth. Fig. 18 presents a series of four satellite images that nicely depict the evolution of the sea surface temperature field and sea ice concentration during the latter part of the event. The locations of the *Healy* XCTD stations are marked in the figure, as well as the two mooring sites (head of Barrow Canyon and Beaufort shelfbreak). Despite the presence of clouds in the images, the signals of interest are easily detected.

The first satellite image is from 10 July 2011, when the ice edge is near the vicinity of the shelfbreak. One sees the presence of warm surface water (ACW) extending to the tip of Pt. Barrow, a good distance along the canyon. The shelfbreak mooring at 152°W is still covered with sea ice at this time. The next satellite image is four days later on 14 July 2011, at which point the warm water has reached the mouth of the canyon. Note also the tongue of warm water extending westward along the Beaufort shelfbreak

past the 152°W mooring site. This is the surface signature of the reversed shelfbreak jet, consistent with the mooring velocity record at 152°W which indicates reversed flow (especially in the upper 50 m) for much of July. It seems likely that the major source of the warm water in the jet was Mackenzie River water entrained into the reversed shelfbreak current (although it is not impossible that some of it is Pacific-origin water that had previously passed by the mooring flowing eastward prior to the wind event). The Barrow wind record indicates that the easterly winds are still strong at this time with peaks over 10 m/s.

The third satellite image is from 16 July 2011 and, although partially obscured by clouds, it clearly shows that the tongue of warm water emanating from Barrow Canyon has turned westward and encountered the ice, appearing to cause considerable melt (although advection of the ice is likely occurring as well). Note that the warm water originating from the east in the Beaufort shelf-break jet has now reached the mouth of Barrow Canyon. The final satellite image is from 19 July 2011. One sees that the warm water continues to progress westward and now intrudes farther into the

basin and into the ice pack, enlarging the area of ice melt. The shelfbreak jet signature remains clear as well.

The *Healy* XCTD section was occupied on 17 July 2011, between the time of the third and fourth satellite images. The temperature and salinity profiles in conjunction with shipboard ADCP measurements allowed for the calculation of absolute geostrophic velocities. The vertical section of potential temperature (Fig. 19a) reveals warm water in the upper layer (as warm as 4 °C) adjacent to the ice edge. The absolute geostrophic velocity section (Fig. 19b) indicates a northwestward-flowing, surface-intensified jet, located well seaward of the shelfbreak. This jet is advecting the warm summer water at speeds greater than 70 cm/s. Shoreward of the jet, and deeper in the water column, is a cyclonic eddy transporting warm water as well. This subsurface feature was likely pinched off of the main canyon outflow via a turbulent process.

Together, the satellite images and the in situ shipboard data provide clear evidence that warm Pacific summer water can be diverted into the interior basin to the west of Barrow Canyon during easterly wind events. This is consistent with the above results

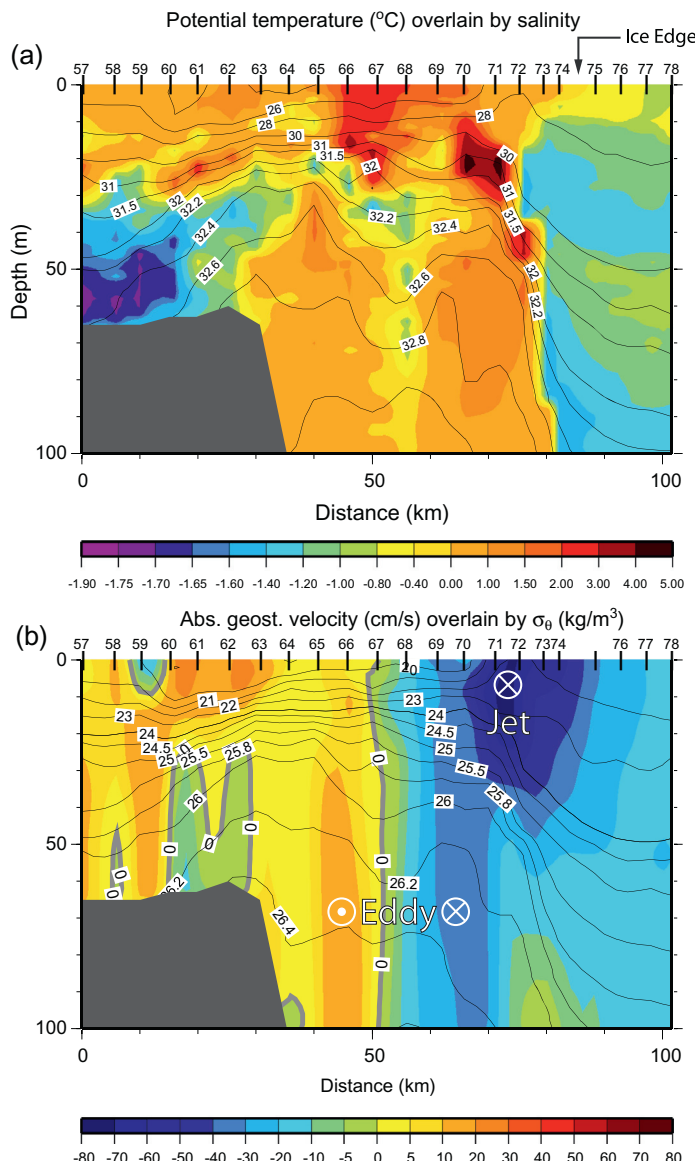


Fig. 19. (a) Vertical section of potential temperature (color, °C) overlain by salinity (contours). (b) Vertical section of absolute geostrophic velocity (color, cm/s) overlain by potential density (σ_0 , kg/m^3). Negative velocities denote flow to the northwest. The locations the XCTD profiles are numbered along the top edge of the plot. The position of the ice edge is indicated as well. (For interpretation of the references to color in this figure legend, the reader is referred to the web version of this article.)

showing that a large portion of the heat reaching Barrow Canyon does not make it into the Beaufort shelfbreak jet during summers with strong easterly winds. It also supports the conclusion that a significant portion of this heat contributes to sea ice melt in the interior basin. Although not shown here, subsequent satellite images indicate that the pack-ice permanently shifted to the north following the two July wind events in summer 2011. We note that the evidence presented here for ice melt via the diversion of Pacific summer water from the Beaufort shelfbreak jet, while compelling, is somewhat anecdotal. Further study is needed to clarify the summer water pathways in the northeast Chukchi Sea as well as the fate of Pacific water in the Canada Basin.

Acknowledgements

The authors thank Dan Torres, Paula Fratantoni, and Frank Bahr for processing the Beaufort Sea mooring data, and Carolina Nobre for providing technical support and assistance with some of the figures. We are grateful to John Kemp, Jim Ryder, and the officers and crew of the USCGC *Healy* and the USCGC *Polar Star* for their hard work during the servicing of the moorings. Support for the most recent deployments of the shelfbreak mooring was provided by Grant # ARC-0856244 from the Office of Polar Programs of the National Science Foundation (EB and RP). Further support for EB was provided by the United States Navy, the National Science Foundation Graduate Research Fellowship Program, and the Woods Hole Oceanographic Institution Academic Programs Office. The Barrow Canyon mooring data was collected as part of the Bureau of Ocean Energy Management study OCS 2012-079.

References

- Aagaard, K., Carmack, E., 1989. The role of sea ice and other fresh water in the arctic circulation. *Journal of Geophysical Research: Oceans* (1978–2012) 94 (C10), 14485–14498. <http://dx.doi.org/10.1029/JC094iC10p14485>.
- Aagaard, K., Coachman, L., Carmack, E., 1981. On the halocline of the Arctic Ocean. *Deep Sea Research Part A: Oceanographic Research Papers* 28, 529–545.
- Aksenov, Y., Ivanov, V., Nurser, A., Bacon, S., Polyakov, I.V., Coward, A.C., Naveira-Garabato, A.C., Beszczynska-Möller, A., 2011. The Arctic circumpolar boundary current. *Journal of Geophysical Research* 116, doi:10.1029/2010JC006637.
- Brugler, E.T., 2013. Interannual Variability of the Pacific Water Boundary Current in the Beaufort Sea. M.S. thesis, Massachusetts Institute of Technology and Woods Hole Oceanographic Institution, Cambridge/Woods Hole, MA.
- Cavalieri, D., Crawford, J., Drinkwater, M., Eppler, D., Farmer, L., Jentz, R., Wackerly, C., 1991. Aircraft active and passive microwave validation of sea ice concentration from the DMSP SSM/I. *Journal of Geophysical Research: Oceans* (1978–2012) 96 (C12), 21989–22008.
- Cavalieri, D.J., Parkinson, C.L., Gloersen, P., Comiso, J.C., Zwally, H.J., 1999. Deriving long-term time series of sea ice cover from satellite passive-microwave multisensor data sets. *Journal of Geophysical Research: Oceans* (1978–2012) 104 (C7), 15803–15814, doi:10.1029/1999JC900081.
- Codispoti, L., Flagg, C., Kelly, V., Swift, J.H., 2005. Hydrographic conditions during the 2002 SBI process experiments. *Deep Sea Research Part II: Topical Studies in Oceanography* 52 (24), 3199–3226, doi:10.1016/j.dsrr.2005.10.007.
- Grumbine, R.W., 1996. Automated Passive Microwave Sea Ice Concentration Analysis at NCEP. Unpublished manuscript available from NCEP/NWS/NOAA, 5200 Auth Road, Camp Springs, MD, 20746, USA, 13pp.
- Itoh, M., Shimada, K., Kamoshida, T., McLaughlin, F., Carmack, E., Nishino, S., 2012. Interannual variability of Pacific winter water inflow through Barrow Canyon from 2000 to 2006. *Journal of Oceanography* 68 (4), 575–592, doi:10.1007/s10872-012-0120-1.
- Kadko, D., Pickart, R.S., Mathis, J., 2008. Age characteristics of a shelf-break eddy in the western Arctic and implications for shelf-basin exchange. *Journal of Geophysical Research: Oceans* (1978–2012) 113 (C2), doi:10.1029/2007JC004429.
- Karcher, M., Kauker, F., Gerdes, R., Hunke, E., Zhang, J., 2007. On the dynamics of Atlantic Water circulation in the Arctic Ocean. *Journal of Geophysical Research* 112, doi:10.1029/2006JC003630.
- Mathis, J.T. et al., 2012. Storm-induced upwelling of high pCO₂ waters onto the continental shelf of the western Arctic Ocean and implications for carbonate mineral saturation states. *Geophysical Research Letters* 39 (7), L07 606, doi:10.1029/2012GL051574.
- Mesinger, F. et al., 2006. North american regional reanalysis. *Bulletin of the American Meteorological Society* 87 (3), 343–360. <http://dx.doi.org/10.1175/BAMS-87-3-343>.
- Moore, G., 2012. Decadal variability and a recent amplification of the summer Beaufort Sea High. *Geophysical Research Letters* 39 (10), L10 807, doi:10.1029/2012GL051570.
- Muench, R., Schumacher, J., Salo, S., 1988. Winter currents and hydrographic conditions on the northern central Bering Sea shelf. *Journal of Geophysical Research: Oceans* (1978–2012) 93 (C1), 516–526.
- Nikolopoulos, A., Pickart, R., Fratantoni, P., Shimada, K., Torres, D., Jones, E., 2009. The western Arctic boundary current at 152°W: structure, variability, and transport. *Deep Sea Research Part II: Topical Studies in Oceanography* 56 (17), 1164–1181, doi:10.1016/j.dsrr.2008.10.014.
- Okkonen, S.R., Ashjian, C.J., Campbell, R.G., Maslowski, W., Clement-Kinney, J.L., Potter, R., 2009. Intrusion of warm Bering/Chukchi waters onto the shelf in the western Beaufort Sea. *Journal of Geophysical Research* 114, C00A11, doi:10.1029/2008JC004870.
- Padman, L., Erofeeva, S., 2004. A barotropic inverse tidal model for the Arctic Ocean. *Geophysical Research Letters* 31 (2), doi:10.1029/2003GL019003.
- Pickart, R., 2004. Shelfbreak circulation in the Alaskan Beaufort Sea: mean structure and variability. *Journal of Geophysical Research* 109 (C4), C04 024, doi:10.1029/2003JC001912.
- Pickart, R., Moore, G., Torres, D., Fratantoni, P., Goldsmith, R., Yang, J., 2009a. Upwelling on the continental slope of the Alaskan Beaufort Sea: storms, ice, and oceanographic response. *Journal of Geophysical Research* 114 (C1), C00A13, doi:10.1029/2008JC005009.
- Pickart, R., Spall, M., Moore, G., Weingartner, T., Woodgate, R., Aagaard, K., Shimada, K., 2011. Upwelling in the Alaskan Beaufort Sea: atmospheric forcing and local versus non-local response. *Progress in Oceanography* 88 (1), 78–100, doi:10.1016/j.pocean.2010.11.005.
- Pickart, R.S., Moore, G., Macdonald, A.M., Renfrew, I.A., Walsh, J.E., Kessler, W.S., 2009b. Seasonal evolution of Aleutian low pressure systems: implications for the north Pacific subpolar circulation. *Journal of Physical Oceanography* 39 (6), 1317–1339, doi:10.1175/2008JPO3891.1.
- Pickart, R.S., Schulze, L.M., Moore, G., Charette, M.A., Arrigo, K.R., van Dijken, G., Danielson, S., 2013b. Long-term trends of upwelling and impacts on primary productivity in the Alaskan Beaufort Sea. *Deep Sea Research Part I: Oceanographic Research Papers*, doi:10.1016/j.dsri.2013.05.003.
- Pickart, R.S., Spall, M.A., Mathis, J.T., 2013a. Dynamics of upwelling in the Alaskan Beaufort Sea and associated shelf-basin fluxes. *Deep Sea Research Part I: Oceanographic Research Papers*, doi:10.1016/j.dsri.2013.01.007.
- Plueddemann, A.J., Krishfield, R., Edwards, C.R., 1999. Eddies in the Beaufort Gyre. *Ocean–Atmosphere–Ice Interactions (OAI)*, All Hands Meeting, 20–22 October, 1999, Virginia Beach, VA.
- Reynolds, R.W., Smith, T.M., Liu, C., Chelton, D.B., Casey, K.S., Schlax, M.G., 2007. Daily high-resolution-blended analyses for sea surface temperature. *Journal of Climate* 20 (22), 5473–5496, doi:10.1175/2007JCLI1824.1.
- Roach, A., Aagaard, K., Pease, C., Salo, S., Weingartner, T., Pavlov, V., Kulakov, M., 1995. Direct measurements of transport and water properties through the bering strait. *Journal of Geophysical Research: Oceans* (1978–2012) 100 (C9), 18443–18457. <http://dx.doi.org/10.1029/95JC01673>.
- Rudels, B., Jones, E., Anderson, L., Kattner, G., 1994. On the intermediate depth waters of the Arctic Ocean. *The Polar Oceans and Their Role in Shaping the Global Environment*, 33–46, doi:10.1029/GM085p0033.
- Schulze, L.M., Pickart, R.S., 2012. Seasonal variation of upwelling in the Alaskan Beaufort Sea: impact of sea ice cover. *Journal of Geophysical Research: Oceans* (1978–2012) (C6), 117, doi:10.1029/2012JC007985.
- Serreze, M.C., Barrett, A.P., 2011. Characteristics of the Beaufort Sea high. *Journal of Climate* 24 (1), 159–182, doi:10.1175/2010JCLI3636.1.
- Shimada, K., Carmack, E.C., Hatakeyama, K., Takizawa, T., 2001. Varieties of shallow temperature maximum waters in the western Canadian Basin of the Arctic Ocean. *Geophysical Research Letters* 28 (18), 3441–3444, doi:10.1029/2001GL013168.
- Shimada, K., Kamoshida, T., Itoh, M., Nishino, S., Carmack, E., McLaughlin, F., Zimmermann, S., Proshutinsky, A., 2006. Pacific Ocean inflow: influence on catastrophic reduction of sea ice cover in the Arctic Ocean. *Geophysical Research Letters* 33 (L08605), doi:10.1029/2005GL025624.
- Spall, M.A., Pickart, R.S., Fratantoni, P.S., Plueddemann, A.J., 2008. Western Arctic shelfbreak eddies: formation and transport. *Journal of Physical Oceanography* 38 (8), 1644–1668, doi:10.1175/2007JPO3829.1.
- Steele, M., Morison, J., Ermold, W., Rigor, I., Ortmeyer, M., Shimada, K., 2004. Circulation of summer Pacific halocline water in the Arctic Ocean. *Journal of Geophysical Research: Oceans* (1978–2012) (C2), 109.
- Steele, M., Zhang, J., Ermold, W., 2010. Mechanisms of summertime upper Arctic Ocean warming and the effect on sea ice melt. *Journal of Geophysical Research* 115 (C11), C11 004, doi:10.1029/2009JC005849.
- von Appen, W., Pickart, R., 2012. Two configurations of the western Arctic shelfbreak current in summer. *Journal of Physical Oceanography* 42 (3), 329–351, doi:10.1175/JPO-D-11-0261.
- Watanabe, E., 2011. Beaufort shelf break eddies and shelf-basin exchange of Pacific summer water in the western Arctic Ocean detected by satellite and modeling analyses. *Journal of Geophysical Research* 116 (C8), C08 034, doi:10.1029/2010JC006259.
- Weingartner, T., Aagaard, K., Woodgate, R., Danielson, S., Sasaki, Y., Cavalieri, D., 2005a. Circulation on the north central Chukchi Sea shelf. *Deep Sea Research Part II: Topical Studies in Oceanography* 52 (24), 3150–3174, doi:10.1016/j.dsrr.2005.10.015.

- Weingartner, T.J., Danielson, S.L., Royer, T.C., 2005b. Freshwater variability and predictability in the Alaska Coastal current. Deep Sea Research Part II: Topical Studies in Oceanography 52 (1), 169–191, doi:10.1016/j.dsrr.2004.09.030.
- Wilson, J.G., Overland, J.E., 1986. Meteorology. The Gulf of Alaska: physical environment and biological resources. In: Hood, D.W., Zimmerman, S.T. (Eds.), Alaska Office, Ocean Assessments Division. National Oceanic and Atmospheric Administration, US Department of Commerce, USA, pp. 31–54.
- Winsor, P., Chapman, D.C., 2004. Pathways of Pacific water across the Chukchi Sea: a numerical model study. Journal of Geophysical Research 109, C03 002, doi:10.1029/2003JC001962.
- Woodgate, R., Weingartner, T., Lindsay, R., 2012. Observed increases in Bering Strait oceanic fluxes from the Pacific to the Arctic from 2001 to 2011 and their impacts on the Arctic Ocean water column. Geophysical Research Letters 39 (24), doi:10.1029/2012GL054092.
- Woodgate, R.A., Aagaard, K., 2005. Revising the Bering Strait freshwater flux into the Arctic Ocean. Geophysical Research Letters 32, doi:10.1029/2004GL021747.
- Woodgate, R.A., Aagaard, K., Muench, R.D., Gunn, J., Björk, G., Rudels, B., Roach, A., Schauer, U., 2001. The Arctic Ocean boundary current along the Eurasian slope and the adjacent Lomonosov Ridge: water mass properties, transports and transformations from moored instruments. Deep Sea Research Part I: Oceanographic Research Papers 48 (8), 1757–1792, doi:10.1016/S0967-0637(00)00091-1.
- Woodgate, R.A., Aagaard, K., Weingartner, T.J., 2005c. Monthly temperature, salinity, and transport variability of the Bering Strait through flow. Geophysical Research Letters 32 (4), doi:10.1029/2004GL021880.
- Woodgate, R.A., Weingartner, T., Lindsay, R., 2010. The 2007 Bering Strait oceanic heat flux and anomalous Arctic sea-ice retreat. Geophysical Research Letters 37, L01602, doi:10.1029/2009GL041621.
- Yang, J., 2006. The seasonal variability of the Arctic Ocean Ekman transport and its role in the mixed layer heat and salt fluxes. Journal of Climate 19 (20), 5366–5387.